GaN-based HEMTs for mm-wave applications

Kathia Harrouche, F Medjdoub

Chapter 3

GaN-based HEMTs for mm-wave applications

Kathia Harrouche and Farid Medjdoub

1. Introduction

Today, the interest for millimeter-wave (mmW) band (30-300 GHz) is continuously increasing, due to its reduced wavelength and wide frequency bands, which enable smaller component with improved performances. Wireless communication systems are extending to higher frequencies as system designers need more bandwidth for many emerging applications. However, several challenges need to be overcome in order to use the mmW spectrum successfully. Monolithic microwave integrated circuits (MMICs) based on III-V semiconductors are the one key to meet the requirements of mmW range. The targeted performances required for high frequency MMICs include the combination high power/high efficiency, compact size and low cost. Gallium nitride (GaN) is one of the most promising semiconductor in this frame.

In this context, this chapter focuses on GaN-based devices for mmW applications. Targeted applications including high power amplifiers, broadband amplifiers and 5G wireless networks are introduced. Various GaN-based material designs for mmW applications are described showing the advantages and limitations for high frequency applications. Device design and fabrication of mmW GaN devices are analyzed. Finally, an overview of MMIC power amplifiers is reported.

2. Targeted applications for GaN millimeter-wave devices

Recent improvements in GaN HEMT devices have allowed the demonstration of a variety of next generation mmW circuits. As introduced in Chapter 1, with its wide bandgap, high saturated electron velocity and higher breakdown voltage, GaN technology is a very promising candidate for realizing circuits with high power, high efficiency and wide operational bandwidth. These advantages are attractive for not only compact solid-state power amplifiers (PAs), but also for the future transmitter design of 5G cellular communications. Figure 3.1 represents the provisional investments on GaN until 2022 for several types of applications. GaN technology investment will continue to grow over time until reaching $ 2.5 billion for the year 2022. Such growth is explained by the fact that GaN will play a major role in many applications and is considered as a strategic technology.

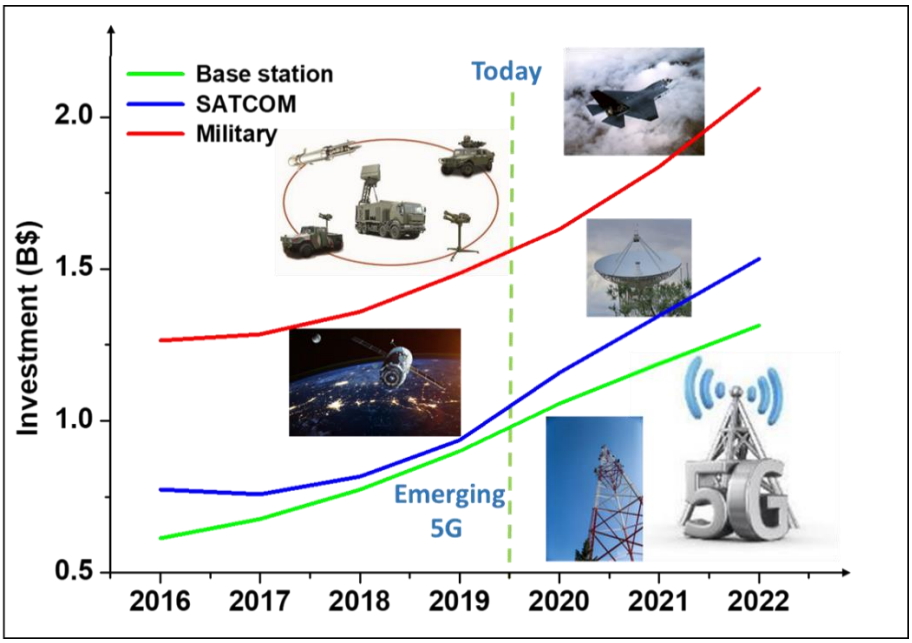

Figure 3.1 Provisional investments on GaN up to 2022 for several types of applications.

2.1. High power amplification

Recent and ongoing progress in semiconductor device fabrication and processing technology has pushed the limits of MMICs for mmW frequencies. MMIC components operating at these frequencies will be used to improve the sensitivity and performance of radiometers, receivers for communication systems and transceivers for radar instruments. The first MMIC was reported in 1976 [1] and progress in output power, gain and operating frequency are continually being achieved afterwards. Latest literature has demonstrated that silicon (Si)-based MMICs such as complementary-metal-oxide-semiconductor (CMOS) Si-On-Insulator (SOI) stacked MMICs, and power-combining Si germanium (SiGe) MMICs, can achieve relatively high power at high frequencies. Consequently, they can be applied to high power applications requiring a few watts below Ka-Band. However, at higher frequencies, Si-based MMICs are limited to deliver the necessary output power compared to GaN-based devices. High power amplifiers have been largely developed in mmW range using other technologies based on III-V materials such as Gallium Arsenide (GaAs) [2][3][4] and Indium Phosphide (InP) [5–7]HEMTs. Despite the excellent achievements, InP and GaAs-based mmW power amplifiers are also limited in saturated power levels due to the low breakdown voltage and related drain bias operation. Advanced GaN HEMTs have demonstrated high power in the mmW range surpassing any other technologies by a factor of 5 to 10 [8]. The superior mechanical robustness as well as the capability to operate at higher temperatures as compared to Si, GaAs and InP materials are additional benefits of GaN [8]. GaN MMICs revolutionize the field of mmW Solid State Power Amplifiers (SSPAs), and enable new applications, that were previously not practical due to the limited output power of SSPAs and large size of Travelling Wave Tube Amplifiers (TWTAs).

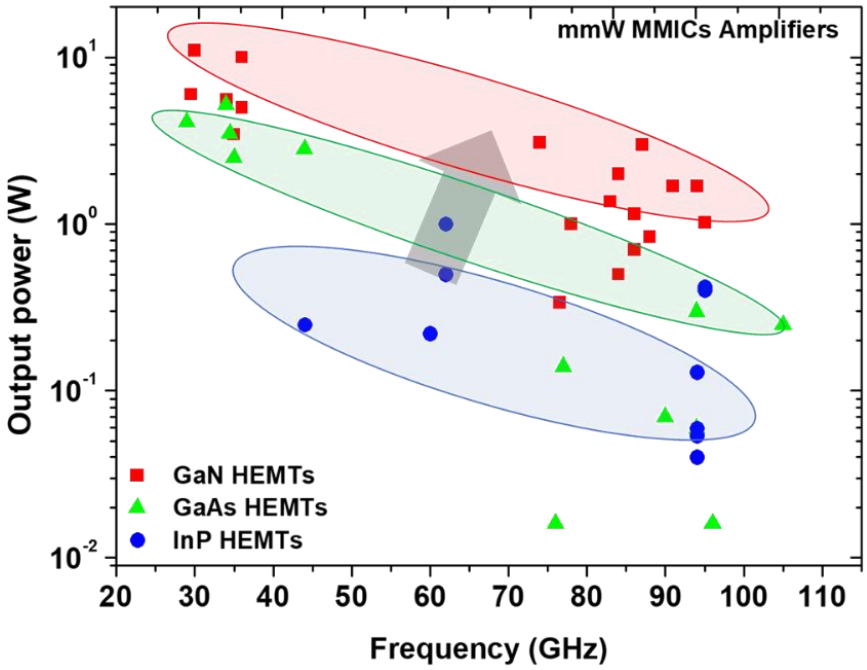

Figure 3.2 Output power of MMIC amplifiers under CW operation based on various semiconductor transistor technologies.

PAs based on GaN HEMT technology operating in mmW frequency range have been demonstrated up to the W-Band. Figure 3.2 shows the main semiconductor technologies and theirs limits in terms of output power and operating frequency. State-of-the-art power level amplifiers have been reported with about 10 W and 3 W at Ka-Band [9][10][11] and W-Band [8][12–20] under Continuous Wave (CW) conditions, respectively. As expected, the output power decreases at higher frequencies due to the device scaling. Indeed, the gate length and the lateral device dimensions (gate-drain distance) are key parameters for high frequency operation. Furthermore, in order to reach high output power density, a high drain voltage is mandatory, which is typically inversely proportional to the device downscaling. On the other hand, spatial power combining enabled 5.2 W output power W-Band GaN MMIC [21]. GaN is well known for its high output impedance and low output capacitance as well as high breakdown voltage. These features lead to high efficiency and high power MMIC performances.

2.2. Broadband amplifiers

In recent years, the application of GaN based mmW MMIC has pushed the state-of-the-art performance of power amplifiers to the next level. For many applications such as instrumentation or communication systems that require the integration of several services with reduced number of components and size, RF power amplifiers covering a wide bandwidth would be highly beneficial. To date, systems covering a wide frequency range require multiple narrowband power amplifiers. These amplifiers are connected by means of switches or triplexers. In either case, losses are introduced by the additional circuity and therefore such a system is not favorable. To reduce costs and system complexity, it is necessary to replace multiple amplifiers by a single broadband power

amplifier covering multiple bands. Wideband power amplifier MMICs based on GaN are thus key components that are employed in numerous applications such as military and wireless communication. For 5G, GaN MMIC PAs are expected to be widely deployed in cellular base stations in order to reduce size and improve system integration. Consequently, it is essential for MMIC implementation to develop low-loss and compact circuits in order to ensure high efficiency and broad bandwidth.

The performance evaluation of power amplifiers is based on five key parameters: Efficiency, output power, linearity, gain and bandwidth. The improvement of power amplifiers has generated significant research and development in recent years. The optimum operation class of power amplifiers depends on the targeted linearity, efficiency and output power. In the conventional operation classes, (A, B, AB and C) the power amplifier operates like a voltage controlled current source. Nevertheless, another aspect that has recently attracted a lot of attention is the enhancement of the amplifier efficiency using the so-called switch-mode concepts such as class D, E and F with the aim of reaching drain efficiencies of 70% and beyond [22].

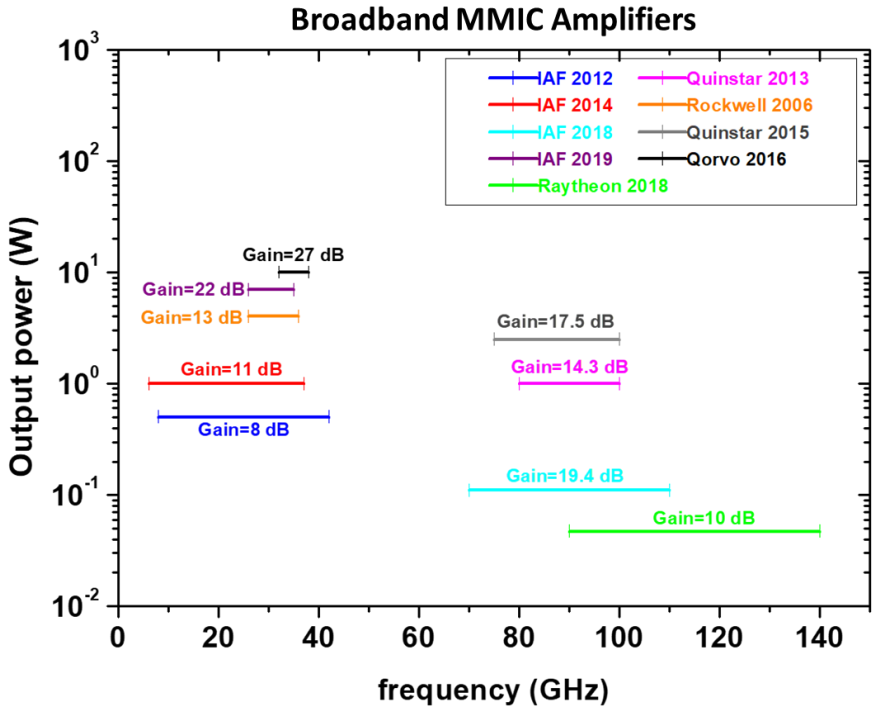

Figure 3.3 Output power of Broadband MMIC amplifiers.

The state-of-the-art broadband high-power mmW GaN MMIC is summarized in Figure 3.3. These results indicate the great potential of GaN-based PAs to increase solid-state power levels while maintaining wide bandwidth. Broadband GaN MMICs have been reported up to 140 GHz with output power ranging from 10 W over 32 – 38 GHz [10] to 47 mW over 90 – 140 GHz [23]. While these MMICs have produced attractive power levels, the highest power level is associated to a much narrower bandwidth as expected. However, by using on-chip traveling-wave power combiner circuit techniques, several watts output power using GaN MMICs have been reported by

Quinstar with a bandwidth approaching the entire W-band [24]. Another reported technology enabling wide bandwidth amplifiers with high gain is the non-uniform distributed power amplifiers (NDPA). In this case, the amplifier uses dual-gate HEMTs in the driver stage of an NDPA, which boost the gain of the overall amplifier at wide bandwidth. IAF reported NDPA MMICs covering a frequency range from 6 – 37 GHz and from 8 – 42 GHz with an output power of 1 W and 500 mW with corresponding power gain above 11 dB and 8 dB, respectively [25][26].

2.3. 5G

The ever-increasing data rate and number of connections for mobile communication offer exciting user experiences in our everyday lives. Currently, the wireless communication frontier is shifting from the current fourth generation (4G) to the forthcoming fifth generation (5G). Major international communication companies and manufacturers are all competing to demonstrate 5G capabilities and features, while simultaneously paving the way for mmW technology. The broadband radio access and wireless networks underline the pioneering aspects of 5G, not only for the telecommunication industry but also for a wide range of vertical sectors, including robotics, automotive, factory automation, healthcare, and education. Although the expected features and use cases for 5G are extensive and diverse, the start of 5G deployment will likely address only a few of the highlighted use cases through three scenarios: ultra-reliable low latency communications (uRLLC), enhanced mobile broadband (eMBB) and massive machine type communications (mMTC) as illustrated in Figure 3.4. Under the 5G umbrella, these scenarios have quite different system-level performance requirements such as latency, mobility, number of users and data rate.

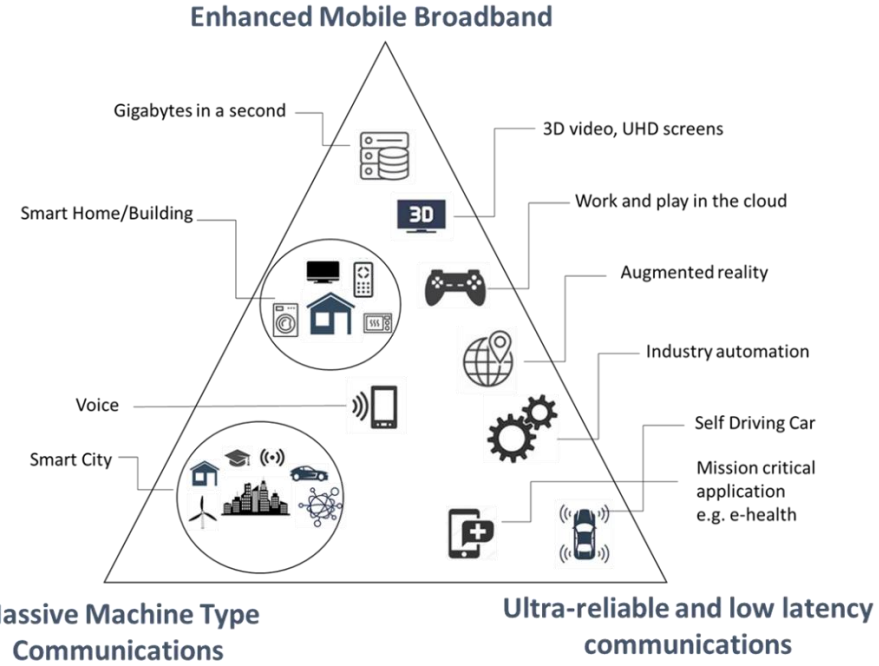

Figure 3.4 Some usage scenarios proposed by International Mobile Telecommunications (IMT)-2020 [27].

The key performance indicators (KPI) for evaluating 5G wireless networks include peak data rate, user experienced data rate, latency, mobility, connection density, energy and spectrum efficiency and area traffic capacity [27]. Table 3.1 summarizes the network features of human-oriented 4G and internet of everything (IoE)-oriented 5G. The targets include the following:

- A peak data rate of at least 20 Gb/s, which is 10 times that of 4G. For some special scenarios such as mmW network backhaul.
- A user experienced data rate of 0.1 Gb/s, which is 10 times that of 4G. In hotspot cases, the user experienced data rate is expected to reach higher values (e.g. 1 Gb/s indoor).
- An energy efficiency of three times and a spectrum efficiency of 10 – 100 times higher compared to 4G.
- An over-the-air latency of 1ms and high mobility up to 500 Km/h. this will provide acceptable quality of service (QoS) for uRLLC scenarios such as automated driving.
- Ten time the connection density of 4G. This will reach up to 10^6 devices/km^2, for example, mMTC scenarios and area traffic capacity of up to 10 Mb/s/m^2.

Table 3.1 The network features of 4G and 5G. VR: virtual reality, AR: augmented reality, UHD: ultra-high definition, V2X: vehicle to everything, IoT: internet of thing, OFDM: orthogonal frequency-division multiplexing, MIMO: multiple input-multiple output, HetNet: heterogeneous network, D2D: device to device, LPDC: low-density parity check codes, SDN: software-defined networking, NFV: network function virtualization.

		4G	5G
Usage Scenarios		• MBB	• eMBB • uRLLC • mMTC
Applications		• High definition videos • Voice • Mobile TV • Mobile internet • Mobile pay	• VR/AR/360° videos • UHD videos • V2X • IoT • Smart city/Factory/Home • Telemedicine • Wearable devices
KPI	Peak data rate	100 Mb/s	20 Gb/s
	Experienced data rate	10 Mb/s	0.1 Gb/s
	Spectrum efficiency	1x	3x that of 4G
	Network Energy Efficiency	1x	10 – 100x that of 4G
	Area traffic capacity	0.1 Mb/s/m²	10 Mb/s/m²
	Connection density	10^5 Devices/km²	10^6 Devices/km²
	Latency	10 ms	1 ms
	Mobility	350 km/h	500 km/h
Technologies		• OFDM • MIMO • Turbo code • Carrier aggregation • HetNet • D2D communications • Unlicensed spectrum	• Mm-Wave communications • Massive MIMO • LDPC and polar codes • Flexible frame structure • Ultra-dense networks • Cloud/fog/edge computing • SDN/NFV/network slicing

- *GaN for 5G*

Compared with current 4G LTE network, the future 5G network for eMBB targets a 20 Gb/s peak data rate, which represents a ten times improvement. New waveforms, along with MIMO, beamforming, and mmW technologies are considered key features for 5G to enable dramatic network performance in terms of both energy and spectrum efficiency. MIMO at mmW frequencies presents major challenges on the hardware design due to the requirements of mmW front-end modules in order to favor beamforming functionality. This poses news challenges in the development of high performances PAs for 5G network. Advanced PAs architectures have evolved with the development of GaN technology to meet ever-greater system level requirements especially in terms of efficiency, power levels and modulation bandwidth. GaN will surpass conventional semiconductor materials for 5G network applications, requiring higher frequencies, tight integration, and minimal implementation cost while operating under harsh environments. These features result in high-efficiency and high power PA performance over a large frequency range, leading to low-cost, large bandwidth, and small size base-station system [28].

- *GaN base station PAs*

To meet the complex requirements of PAs for 5G applications, the device technology selection as well as the circuit configuration are critical. Several key directions for 5G have emerged. In turn, Silicon still wins in the sub-6 GHz, but at higher frequencies, GaN is increasingly attractive. On the other hand, the critical allocation of spectrum will dictate the design and implementation of transceiver hardware. However, the available spectrum for high data rates is limited to the microwave range. That is why, mmW frequencies are necessary extend the current 4G frequency bands. Recently, various GaN PAs have been reported in this frame. Modulated signals with higher bandwidth and a more complex scheme are used to realize greater data rate. Moreover, the demand is increasing for efficiency under multiband, multimode operation. Various approaches such as Doherty amplifiers, Envelope tracking amplifiers and a digital transmitter based on GaN have been demonstrated [29][30][31]. While mmW 5G is being developed, it will be first implemented on sub-6 GHz 5G systems using the same MIMO beamforming techniques but at lower, more technologically accessible frequencies [32]. 5G communication network is designed not only for spectrum bands below 6 GHz but also for high bands above 24 GHz (mmW). A number of sub-6 GHz 5G MIMO systems have been demonstrated at 3.3, 4.2 and 2.14 GHz [32][33]. In the mmW, several GaN PAs have been proposed. Table 3.2 summarizes some performance results of PAs at different frequencies especially in Ka-band for 5G applications.

With the increasing need of data rates, modern communication networks use high bandwidth modulation schemes with high power average ratio (PAR) but at the expense of PA efficiency. At high PAR, the PA must be operated with significant back-off from its saturation point in order to

achieve the required linearity at the PA output. Furthermore, the PA maximum output power level must be reduced so that the entire signal is within the linear region thus decreasing the efficiency [34]. A solution is the use of advanced PA architectures in order to enhance the PA efficiency while maintaining high linearity. Examples would be Doherty, envelope tracking (ET), outphasing and switch mode PAs based on class-D and class-S amplifiers.

Table 3.2 Performance comparison of different PAs for 5G applications. [29][32,34–38].

Reference	Type	Size	f (GHz)	P_{out} (dBm)	PAE (%)	PAR (dBm)	Gain (dB)
[27]	PA	2.9 mm x 1.7 mm²	26.5 – 29.5	36.9 to 38	17.9 to 23	NA	NA
[30]	Doherty PA	1.8 mm x 1.7 mm	28	36	51	NA	30
[32]	Switching mode PA	NA	28 – 39	24.3	59	NA	8.2
[33]	PA	3.8 mm x 6.2 mm²	26 – 28	43.3 to 41.6	19.8 to 13.2	NA	NA
[34]	HPA	3.4 mm x 3.3 mm	26.5 – 29	39	25	NA	21.1 to 24
[35]	Doherty	3.4 mm x 2 mm²	23	36.9	27	29.4	15.4
[36]	Doherty PA	2.7 mm x 1.6 mm²	27.5 – 29.5	35.6	25.5	NA	NA

The Doherty PA technology, which uses active load modulation, is a promising architecture to enhance efficiency and linearity at back-off operation. Doherty amplifiers covering multiband frequency range using GaN technology have been demonstrated with high efficiency up to Ka band [32,34,38,39]. In addition, envelope tracking PAs based on dynamic modulation are also competitive to increase PA efficiency. In this case, to maintain high efficiency in the back-off region, the envelope amplifiers dynamically modulate the supply voltage of the RF PA. Both advanced PA architectures will continue to dominate RF and mmW applications requiring multiband and high efficiency for 5G applications. Nevertheless, bandwidth and linearity are still one of the most important limitations in the Doherty and ET PA techniques. To overcome these issues, several techniques have been proposed, including digital predistorsion technique (PDP) [34][40]. The other recent progress in this frame is the linear-amplification-using-non-linear-components (LINC) outphasing PA architecture, which is attractive for 5G systems because of its strong potential to provide high efficiency with a large peak to PAR signal [41]. Despite the proposed approaches, there are a large room for improvement of PA performances in order to satisfy such practical requirements of 5G wireless communication network, such as mmW, high linearity, high output power, large bandwidth and compact size. GaN HEMTs are among the most suitable devices for power amplifiers and will certainly play a major role as broadband technology for 5G wireless communication.

- *Moving forward to 6G*

The 5G network system has been defined as the key for IoE application. Research efforts invested in mmW wireless communications and the success of 5G preliminary tests ensure that the commercialization and first deployments of 5G wireless networks are expected to ramp up during 2020 [27]. The promised groundbreaking of 5G system operating essentially at high-frequency between 24 and 71 GHz, will solve the spectrum deficit in 4G cellular communication systems currently limited to sub-6 GHz frequencies. Although, the 5G systems that are being marketed will support basic IoE application, the increasing number of new applications such as wireless backhaul, VR/AR and space travel makes it questionable whether they can satisfy emerging services and newer applications that have not been conceived yet. This creates a motivation towards sixth generation (6G) networks.

Recent investigations have identified the key enabling technologies that might define the 6G. Future 6G wireless communication will be implemented in about ten years (2030) [42] with devices operating up to the THz range. The key figure of merits for the evaluation of 6G wireless networks include a peak data rate of 1 Tb/s, which is 100 times that of 5G, a latency of 10 – 100 μs, an energy efficiency of 10 – 100 times better than 5G. The level of 6G maturity reachable in ten years by sub-THz can make this technology a powerful enabler.

3. GaN-based material designs for mm-Wave applications

Historically, advances of semiconductor technologies based on MMICs have led to continuous performance improvements. GaN represents a leap ahead as compared to other technologies for many RF applications. In early 1990s, GaN has been recognized as a potential solution to satisfy the combination of high power and high frequency requirements [43].

3.1. Intrinsic characteristics and comparison with other materials for RF devices

Figure 3.5 shows the material properties of widely used mmW semiconductors, demonstrating advantages of GaN based material system for high frequency and high power applications. Because of its excellent properties, GaN technology is recognized as a revolutionary material with a wider energy gap of 3.4 eV that exceed 3 times those of InP, GaAs and Si thus allowing higher breakdown voltage and higher operating voltage. The high-saturated electronic velocity of 2.5×10^7 cm/s is another attractive characteristic of GaN. The electron velocity is related to the current density, thus GaN is able to produce high current at high voltage. Since power is a function of voltage and current, the wide energy gap and the high electron velocity allow for ideal high power devices. Moreover, as described in Chapter 1, GaN-based heterostructures deliver a high electron mobility of $1\text{-}2\times10^3$ cm²/Vs, which allows low on resistance. Therefore, high power added efficiency (PAE) can be achieved at high frequencies. GaN thermal conductivity (in the range of 1-3 ÷ 2.1 W/cm.K) is much higher than GaAs and InP. The thermal conductivity is a key factor directly related to the power dissipation from the device. The comparison of the various materials

using the Johnson figure of merit (JFoM) clearly demonstrates the superiority of GaN HEMTs over its counterparts [44][45].

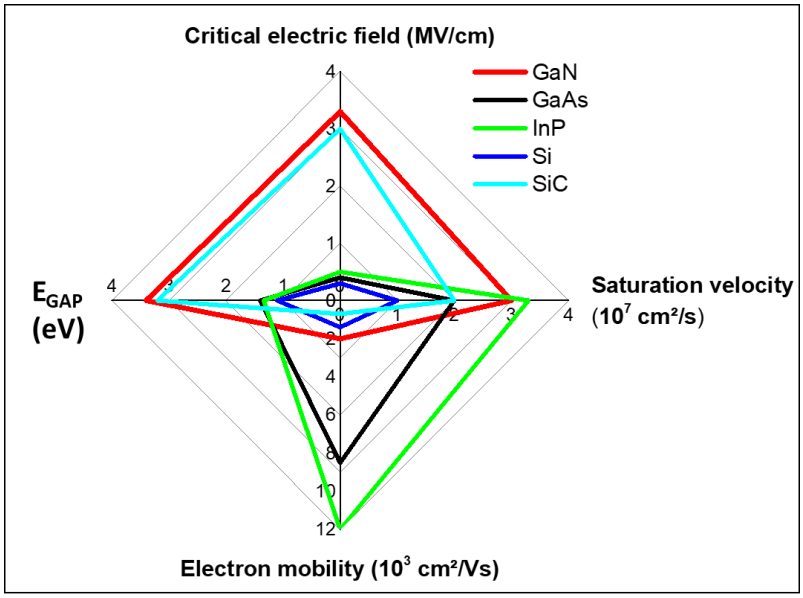

Figure 3.5 Material properties for millimeter-wave semiconductors.

In addition to the device performances, the associated reliability is crucial. For short devices delivering high performances at high drain bias, the main limitation is the device reliability due to a significant electric field peak and subsequent high junction temperatures. It can be pointed out that the so-called field plates have been successfully implemented in the microwave range to ensure high device reliability by spreading the electric field peak. However, this approach cannot really be used for mmW devices due to high induced parasitic capacitances degrading the gain. Assessing the reliability at an early stage of a technology development is of prime importance. Tests are typically carried out under specific operating and environmental conditions (such as temperature, voltage, current…) in a given time duration. The reliability and performance under high temperature conditions have been studied [46]. GaN mmW HEMTs can provide stable device performance up to high junction temperature [47–52]. Figure 3.6 shows an example of RF monitoring performed at 40 GHz on a promising AlN/GaN HEMT structure with a gate length L_g = 110 nm and gate to drain distance L_{gd} = 1.5 µm. The devices have been tested during 24 hours up to a base-plate temperature of 140°C (corresponding to a junction temperature above 250°C) by steps of 4 hours at V_{DS} = 20V. A high PAE (50%) with a P_{OUT} around 3 W/mm at 40 GHz remains stable (Figure 3.6a) with no increase of gate and drain leakage currents (Figure 3.6b).

GaN is well suited not only for high power and high frequency, but also lead to smaller and cheaper chip size. The GaN MMICs reported so far have more than 5 times higher power density with smaller size than GaAs MMICs [15][48][53]. As illustrated in Figure 3.7, GaN MMICs can be reduced by 82% as compared to GaAs pHEMT MMIC while providing more than 4 times power density. As a result, GaN MMICs can deliver higher efficiency due to the reduced on-chip

combining losses both at the MMIC and module levels. That is why, GaN MMICs will revolutionize the field of mmW SSPAs and enable new applications, that were previously not practical due to limited power of SSPAs or large size and high cost of TWTAs.

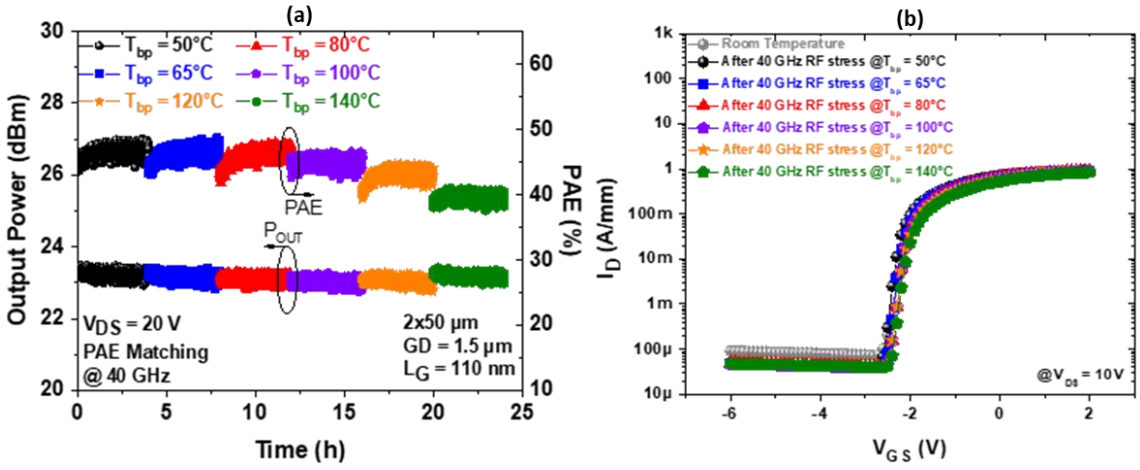

Figure 3.6 (a) Output power and PAE monitoring for 24 hours up to140°C, (b) transfer characteristics before and after the stress [50].

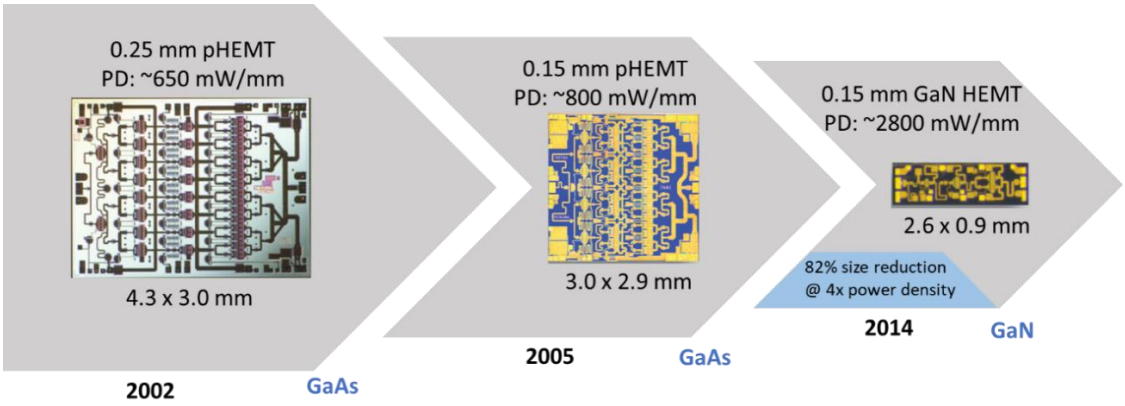

Figure 3.7 MMICs comparison with different technologies.

However, GaN HEMTs are still plagued by two important phenomena, especially when reducing the device dimension: the trapping effects and the self-heating, which can directly cause current collapse and kink effect thus reducing the device performances [54][55]. Trapping effects that occur at different location of the devices are mostly related to the crystalline imperfection induced during growth and device processing as shown in Figure 3.8a. Surface [56][57] or buffer trapping [58] is generally electric field dependent. Several techniques are used to assess the trapping effects such as deep level transient spectroscopy measurements [59][60], temperature dependent threshold voltage analysis [61] or pulsed measurements [50][59][62]. As shown in Figure 3.8b, pulsed I-V

characteristics performed with quiescent drain voltages up to 25V at V_{GS} = +2V of AlN/GaN HEMT devices show rather strong trapping effects as seen from the gate and drain lag due to the residual surface and buffer traps.

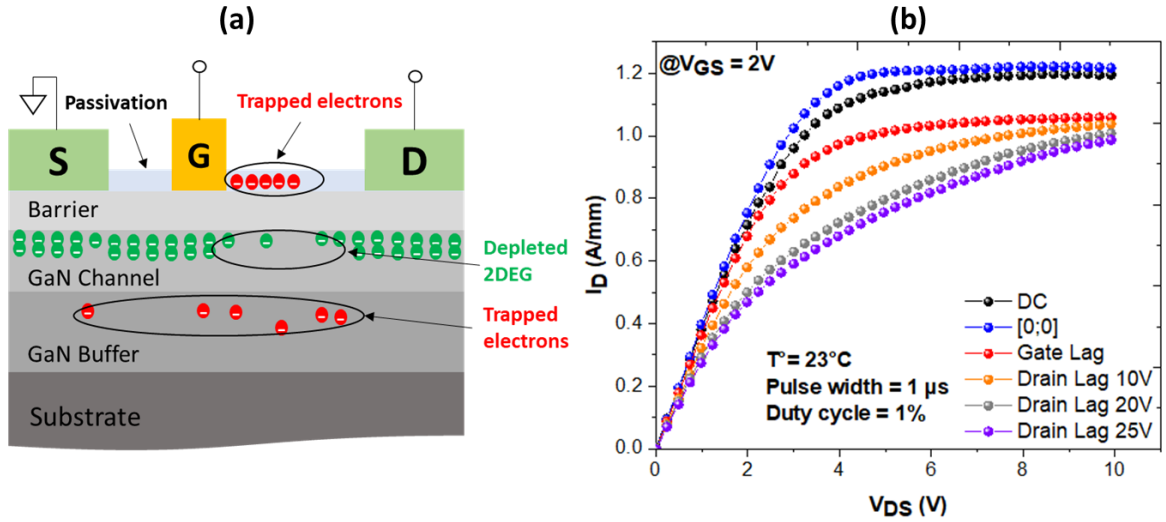

Figure 3.8 Schematic cross section of AlN/GaN HEMT, showing electron trapping location (a), Pulsed I_D-V_{DS} characteristics with various quiescent bias points: Cold point: V_{DS0} = 0V, V_{GS0} = 0V, gate lag: V_{DS0} = 0V, V_{GS0} = -6V and drain lag: V_{DS0} = [10V-25V], V_{GS0} = -6V (b) [50].

The trapping/de-trapping mechanisms induce electrical parasitic effects such as current collapse and kink effect are shown in Figure 3.9a. Several investigations have demonstrated that current collapse effects is related to the presence of traps and hot electron injection into the buffer layer under high electric field [55]. It was also shown that the current collapse is attributed to trapping under the gate and in the gate-drain access region using photo-transient measurements [63]. Another electrical parasitic effect due to the trapping mechanism is the kink effect that increases the drain current, resulting in a shift of pinch-off voltage towards more negative voltages. Several explanations have been suggested [64]: the impact ionization and subsequent hole accumulation causing the change of surface or channel/substrate interface, field-dependent trapping/detrapping in deep levels [65] and a combined effect of impact ionization and deep levels which induce a modification of surface states, buffer or channel/substrate interface deep levels by the generated holes [66]. Other studies have reported that kink effects in GaN HEMTs are related to both impact ionization coupled with the presence of slow traps in the epitaxial layers under the gate, possibly into the GaN buffer [67][68].

Figure 3.9b shows a comparison between large signal CW and pulsed mode at 40 GHz of output power density, PAE and small signal gain as a function of V_{DS} of AlN/GaN HEMTs. The gap in terms of performances between CW and pulsed mode, especially for the PAE confirms the presence of traps within these devices. That is why, the optimization of material quality, and related process technology is necessary in order to minimize the trapping effect phenomena. Many efforts have been carried out to minimize the parasitic effects due to electron trapping such as:

- The use of silicon nitride passivation (Si_3N_4) to improve the gate lag [54][59][69],
- The optimization of epitaxial growth conditions in order to suppress deep level traps into the buffer layers [70],
- The use of gate field plates technology to spread the electric field in the vicinity of the gate [71] or the use of an in-situ SiN passivation reducing drastically the surface states are key parameters to improve RF performances.

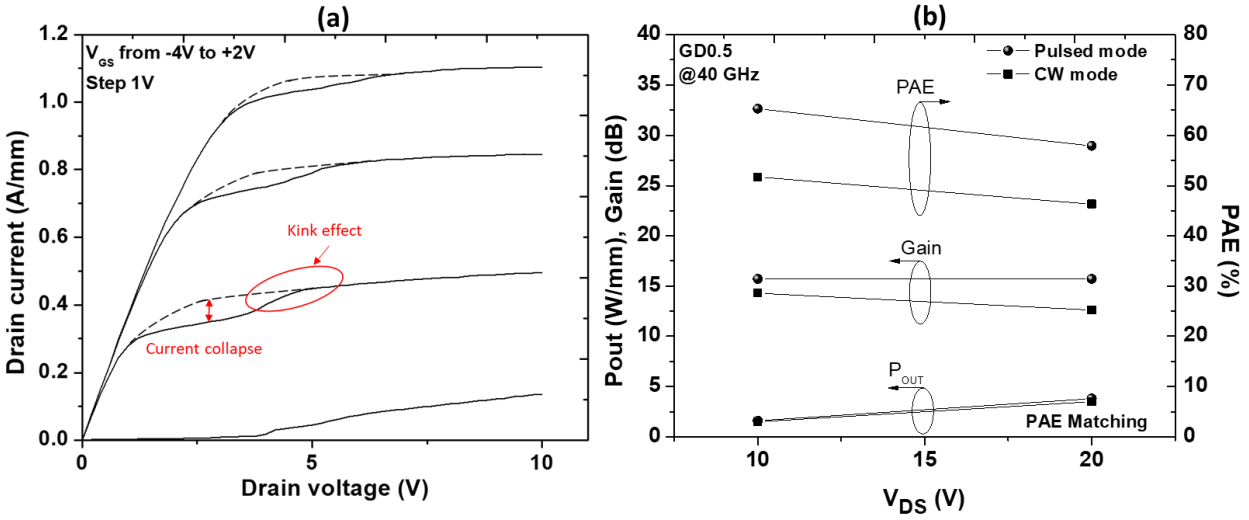

Figure 3.9 I-V characteristics showing the current collapse and kink effects due to electron trapping (a) and CW (circle) and pulsed (square) output power density, PAE and small signal gain as a function of V_{DS} at 40 GHz of AlN/GaN HEMTs (b) [50].

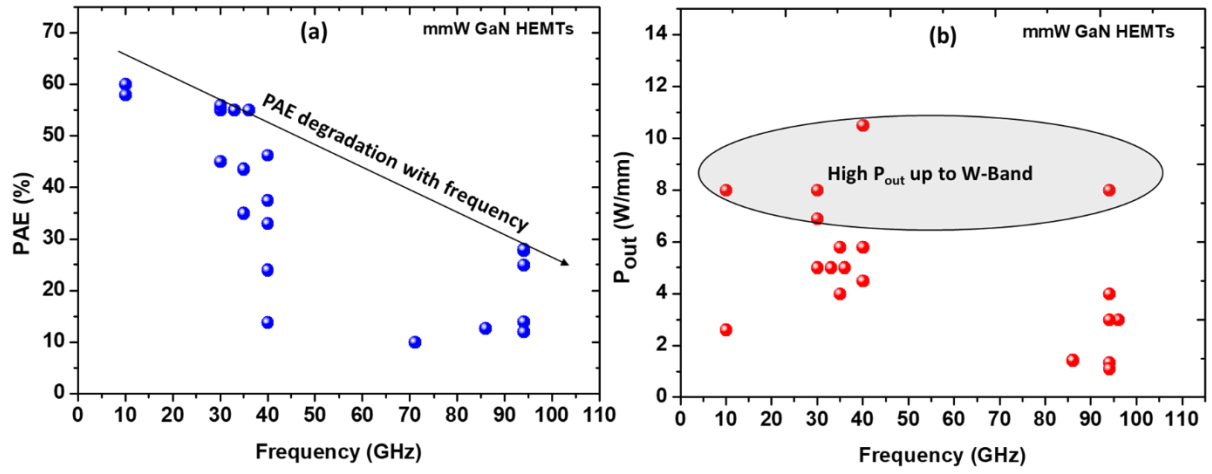

Figure 3.10 PAE (a) and associated Output Power Density (P_{out}) (b) of GaN HEMTs versus the frequency of operation.

High frequency operation requires aggressive device scaling to increase the gain and the frequency performances of GaN HEMTs. Figure 3.10 shows a benchmark of PAE and P_{OUT} of GaN HEMTs

as a function of frequency. Very high efficiency up to 60% and P_{OUT} up to 8 W/mm at Q-band have been reported [50]. However, at higher frequency, the efficiency of GaN HEMTs is still limited mainly due to an insufficient gain. At W-band, the highest PAE reported to date is 27.8 % [72]. As shown in Figure 3.10a the PAE decreases with the frequency while P_{OUT} remains above 8 W/mm (Figure 3.10b). The major current challenge for mmW GaN based devices is to maintain high PAE at high frequencies together with strong robustness.

On top of trapping enhancement and limited PAE, the device scaling can directly affect the breakdown voltage (V_{BK}) due to the reduction of the gate-to-drain distance [73]. Figure 3.11 shows the three terminal breakdown voltage as a function of L_g for different L_{gd}. The plot demonstrates that L_{gd} has more impact on the breakdown voltage than L_g. Therefore, high breakdown voltage can still be maintained with short devices by using proper device designs.

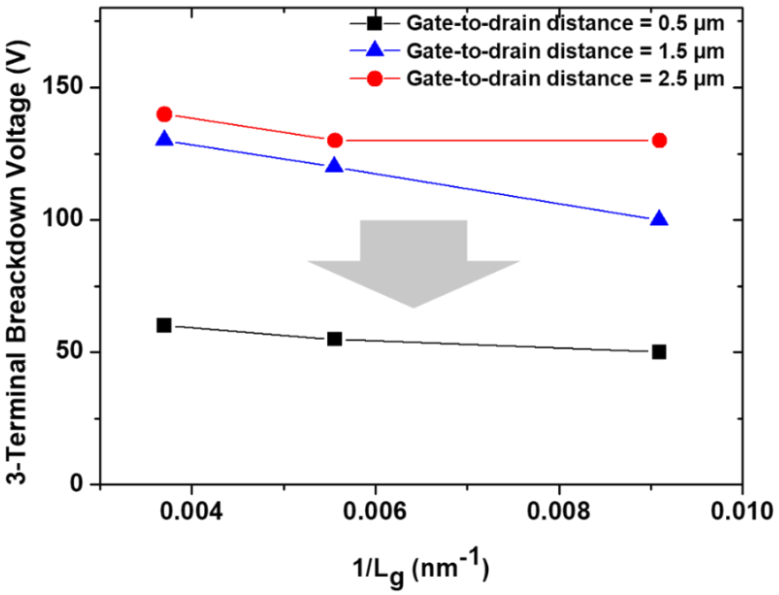

Fig 3.11 3-Terminal Breakdown Voltage of AlN/GaN HEMTs as a function of gate length and gate-to-drain distance (0.5 µm and 1.5 µm).

Today, GaN HEMTs are the most attractive electronic devices for high power mmW applications owing to their intrinsic properties. High power and high frequency GaN HEMT performances are continuously improving in the mmW range. Nevertheless, the robustness and subsequent reliability remain under investigation as both scaled material and devices need to demonstrate high stability, reproducibility and uniformity.

3.2. Specific material systems for RF devices

GaN HEMT epitaxial heterostructures based on III-Nitride materials consist of a wide bandgap barrier layer (AlN, InAlN, InAlGaN or AlGaN), a GaN channel and GaN-based buffer layers grown on top of a substrate using Metal Organic Chemical Vapor Deposition (MOCVD) or

Molecular Beam Epitaxy (MBE). GaN-based HEMTs are typically grown as follows from bottom to top:

- Nucleation layer: typically based on AlN, which is essential in order to accommodate the lattice mismatch between the buffer and the substrate enabling high quality GaN hetero-epitaxy.
- GaN buffer layers: should be of high quality to avoid deep trap levels and lead to a high electron confinement into the channel by using a back barrier or by incorporating acceptor type dopants such as carbon (C) or iron (Fe) in order to increase the resistivity.
- GaN channel: generally undoped to allow high electron transport quality, the channel thickness is part of a trade-off between the electron confinement and the trapping effects.
- Barrier layer: AlGaN-based for microwave devices and preferably ultrathin Al-rich materials for mmW range in order to avoid gate recess, which can compromise the device reliability. The thickness and alloy composition are key parameters to mechanical strain and piezoelectric polarization, defining also the two-dimensional gas (2DEG) density [74].
- SiN cap layer: enables to prevent the stress relaxation of the hetero-interface Al-rich barrier/GaN channel, and passivate the surface states in order to reduce the DC to RF dispersion [75][76].

Figure 3.12a shows an example of an AlN/GaN HEMT cross section consisting in 10 nm SiN cap layer, 3 nm AlN ultrathin barrier, 100 nm GaN channel, a carbon-doped GaN buffer, and an AlN nucleation layer grown on SiC substrate. Figure 3.12b reveals the transmission electron microscopy (TEM) of this structure by MOCVD grown.

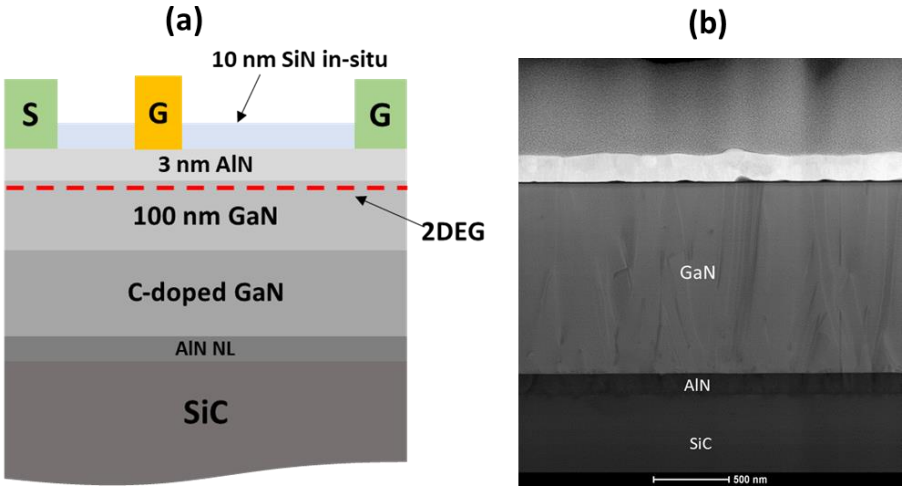

Figure 3.12 Cross section (a) and transmission electron microscopy (TEM) of the MOCVD grown AlN/GaN/SiC with 3 nm AlN barrier (b).

The high spontaneous polarization between GaN and AlN lead to a significant sheet carrier density [77], which combined to a gradient in alloy composition at the barrier/channel interface yields an increasing amount of free carrier into the barrier layer. This results in a strong electron scattering and a reduction in the 2DEG mobility [78]. Figure 3.13 shows the electrical properties of GaN

HEMT structures based on different barrier layers grown on SiC substrate. Room temperature Hall measurements shows that the high sheet charge density of 1×10^{13} cm^{-2} obtained using an AlGaN barrier layer can be increased to 1.9×10^{13} cm^{-2} for an AlN barrier layer. Moreover, the 2DEG mobility decreases as expected with the increase of the sheet carrier density from more than 2000 $cm^2/V.s$ for rather low Al content (<25%) AlGaN barriers to about 1000 $cm^2/V.s$ for AlN barrier layer.

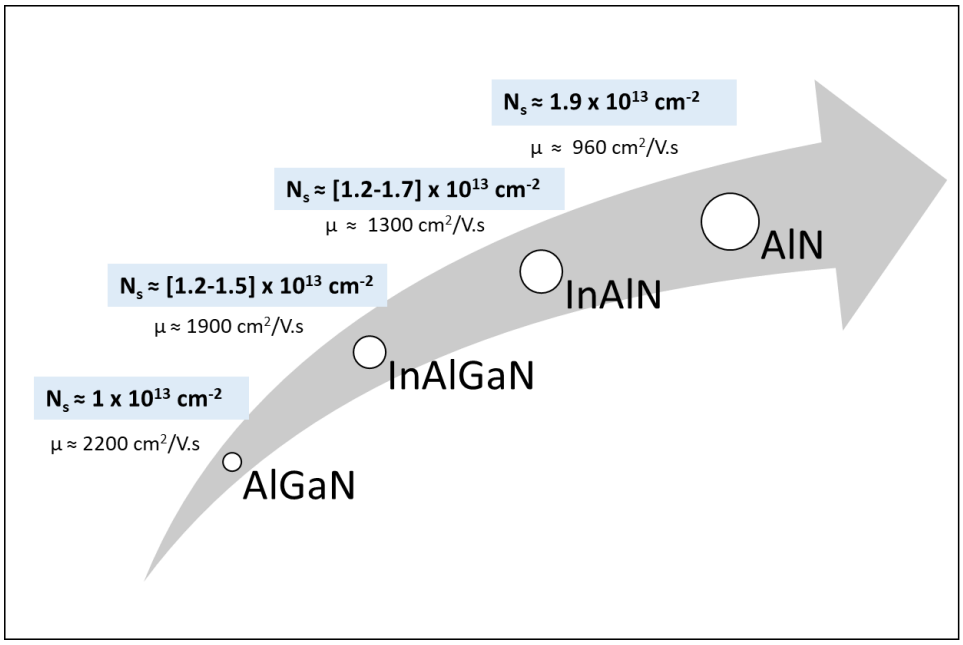

Figure 3.13 2DEG properties for different barrier layers.

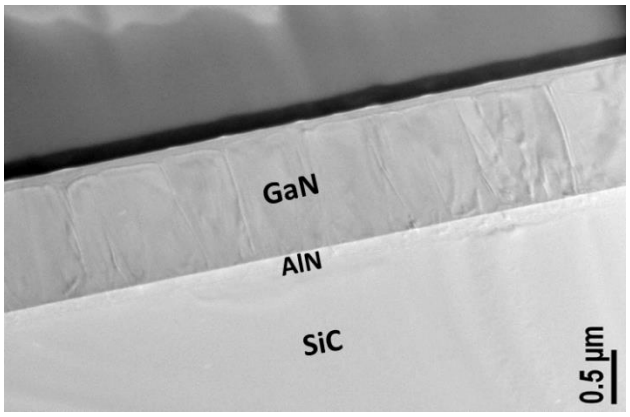

Figure 3.14 TEM image of GaN grown on SiC.

As introduced in Chapters 1 and 2, an important aspect of GaN technology is the substrate material. The choice of substrate depends on the available size, cost, thermal conductivity, coefficient of thermal expansion (CTE), lattice mismatch and targeted applications. Since bulk GaN substrates are still unavailable on large wafer diameter, GaN HEMTs are typically grown on SiC, Si and sapphire. However, Sapphire has a low thermal conductivity with CTE and lattice constant

showing a significant mismatch with GaN. Si substrates present many advantages such as compatible processing with advanced CMOS, availability of large wafer diameter and an acceptable thermal conductivity. Nevertheless, it also suffers from a large lattice mismatch with GaN as reflected by dislocations. Recent reported data confirm that SiC is the most attractive substrate for GaN mmW power devices, because of its low lattice mismatch with GaN and high thermal conductivity enabling superior power operations that are not reachable by any other materials. Figure 3.14 shows TEM image of GaN grown on SiC showing a rather low dislocation density.

4. Device design and fabrication of mm-Wave GaN devices

4.1. Description of key processing steps for various GaN device designs

- *Device scaling for millimeter-wave*

GaN HEMT device scaling is required in order to enhance the high frequency performances. These optimizations are needed not only for the epitaxial structure but also for some processing steps such as ohmic contacts, and gate module. The electron transit time is reduced by using shorter gate lengths, however, a high aspect ratio L_g/a (gate length/gate-to-channel distance) above 15 combined with a high carrier density N_s should be maintained [79]. This allows preventing short channel effects while improving the F_t/F_{max} ratio that are defined by the following equations:

$$F_t = \frac{g_m}{2\pi(C_{gs}+C_{gd})}, \quad F_{max} = \frac{F_t}{2\left(R_g+R_{ds}\right)^{1/2}}$$

where g_m, C_{gs}, C_{gd}, R_g and R_{ds} are transconductance, gate-to-source capacitance, gate-to-drain capacitance, gate resistance and drain-to-source resistance, respectively.

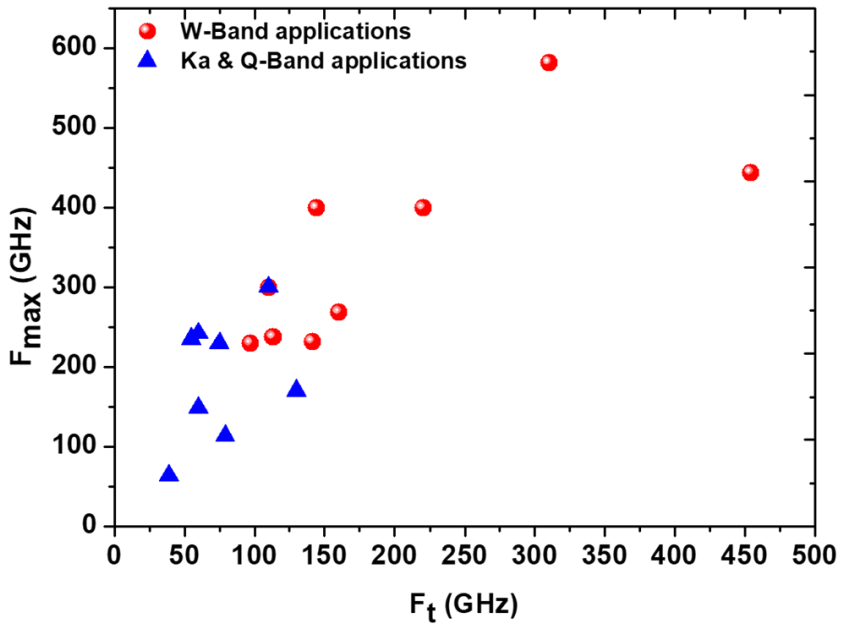

Figure 3.15 Maximum oscillation frequency (F_{max}) as a function of cutoff frequency (F_t) of GaN HEMTs.

To increase F_{max}, each parameter including F_t and parasitic elements such as R_g and C_{gd}, needs to be optimized. Following many efforts from the research community, the best F_t and F_{max} reported to date are about 450 GHz (Figure 3.15). These performances have been achieved through innovative device technologies such as T-shaped gate [80], n^+ GaN ohmic contact regrowth [81], self-aligned gate process [82], vertically scaled epitaxy [80].

- *T-shaped gate design*

T-shaped gates are widely used for achieving both low gate resistance and parasitic capacitances when reducing the gate length [83]. Parasitic elements become of paramount importance with shorter devices. As a matter of fact, the frequency performances are currently mainly limited by the short channel effects and parasitic elements. Figure 3.16a shows the schematic cross section of a GaN HEMT illustrating the parasitic elements and the benefits of the T-gate with reduced gate length, which basically enabled to achieve high RF performances [80]. Moreover, the reduction of the gate length led to a significant increase of F_t up to 450 GHz with a gate length of 40 nm as shown in Figure 3.16b.

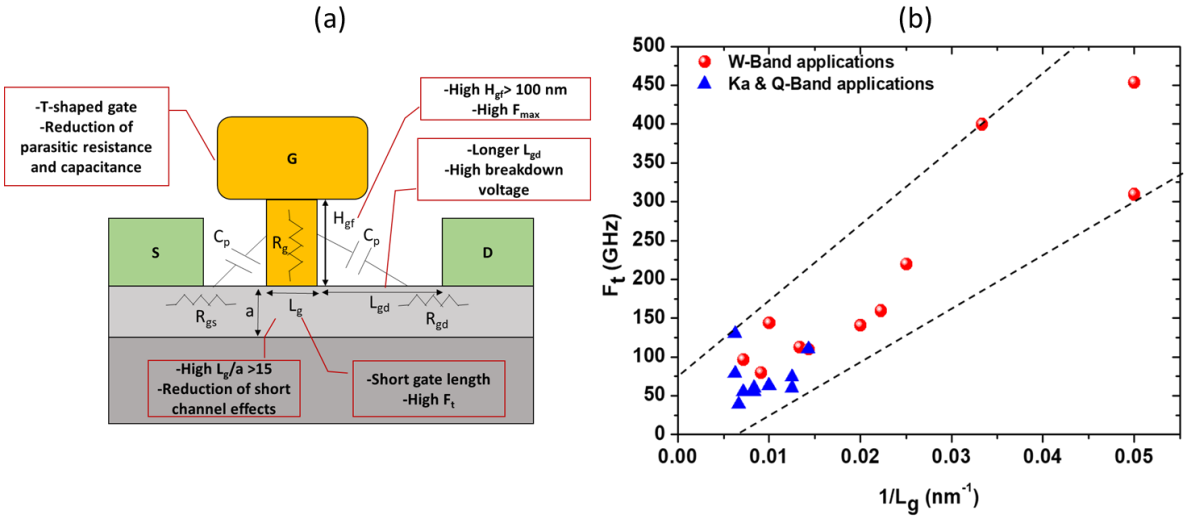

Figure 3.16 Cross section of T-gate GaN HEMT (a) and Scaling of cutoff frequency (F_t) of GaN HEMTs with the gate length (L_g) (b).

- *Advanced ohmic contacts technology*

For millimeter-wave applications, low contact resistances are mandatory to minimize total parasitic resistances and enhance the device performances. Nevertheless, a low contact resistance is difficult to achieve because the wide bandgap of III-nitride HEMT heterostructures. Moreover, the high potential of barrier layer, especially when using high Al content may lead to high contact resistances [84].Conventional planar ohmic contacts are the simplest and low cost method, which

are formed by alloying a complex metal stacks followed by an annealing at an optimum temperature. However, high temperature annealing generally results in severe lateral ohmic metal diffusion as well as rough metal surface. Typical contact resistances are about 0.25 to 0.5 Ω.mm leading to high parasitic resistances proportional to the device scaling. Several approaches have been studied in order to successfully reduce the contact resistance such as: recessed ohmic contacts enabling lower temperature and thus better contact definition [85][86], ion implantation prior to the metallization [87], face treatment [88] and regrown ohmic contacts by MBE technique [80]. Among these approaches, regrown n^+-GaN ohmic contacts is the most promising technology to minimize parasitic access resistances. The ohmic contact regrowth approach enables direct contact between n^+-GaN and 2DEG layers that results in low interface resistance [82]. Very low contact resistances are demonstrated [89][90]. As expected, the combination of high electron mobility and high sheet carrier density reduce the access resistances where the gate-to-source distance needs to be reduced leading to excellent device performances. This makes such a design attractive for millimeter-wave applications.

- *N-polar GaN HEMTs*

The conventional GaN HEMTs are generally developed with a Ga-polar orientation where the 2DEG is formed at the barrier layer/channel interface while the polarization is inverted in N-polar heterostructures as shown in Figure 3.17. The N-polar structure presents several advantages such as low contact resistances due to the 2DEG induced above the hetero-interface and an excellent electron confinement owing to the back barrier under the channel.

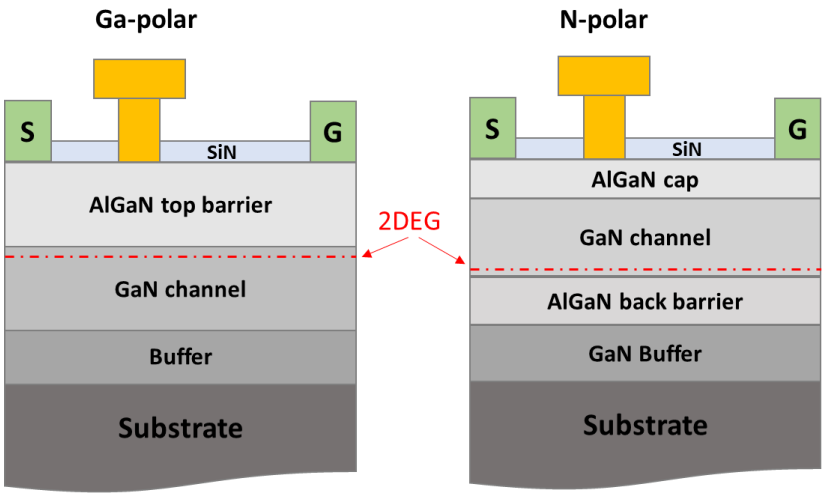

Figure 3.17 Device schematic cross section of Ga-polar and N-polar HEMTs.

Development of N-polar GaN devices and recent results reported by University of California, Santa Barbara (UCSB) show large potential for improvements in the mmW power applications. *Wienecke et al.* reported an output power density of 6.7 W/mm with a PAE of 14.4% at 94 GHz using N-polar GaN cap MISHEMT with a deep gate recess in order to control the dispersion [91]. Using a self-aligned gate to recess, *Romanczyk et al.* demonstrated high breakdown voltage and

high power density of 8 W/mm associated to a PAE of 28% at 94 GHz [92]. It can be noticed that the device robustness under harsh conditions still need to be demonstrated with this configuration system.

- *AlN-based devices performances*

Figure 3.18 shows the epitaxial structure and the schematic cross section of Hughes Research Laboratories (HRL) fourth generation asymmetric self-aligned T-gate GaN HEMTs. The gate length was 20 nm and the ohmic contact regrowth technique is used which allows direct contact of n^+-GaN to the 2DEG enabling extremely low interface resistance of 0.026 Ω.mm. An ultrathin sub-5 nm AlN barrier is used, which delivers high electron density n_S while maintaining a high aspect ratio L_g/a. The asymmetric self-aligned gate with L_{gs} = 30 nm and L_{gd} = 80 nm allows high speed with a breakdown voltage of 17V. This results in a high RF performance reflected by an F_t of 454 GHz and an F_{max} of 444 GHz [93]. The same device with a gate length of 40 nm achieved high large signal performances at W-band. Output power was 1.37 W associated to a PAE of 27% at 83 GHz [19]. Furthermore, graded-channel AlGaN/GaN HEMT demonstrated a large potential to operate at mmW range. 30 GHz large signal measurements showed an excellent PAE of 72% with an output power of 2 W/mm [94].

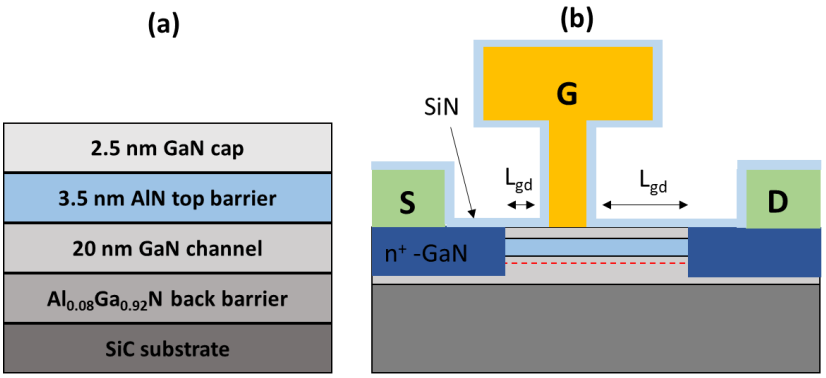

Figure 3.18 Epitaxial structure (a) and schematic cross section of the AlN/GaN HEMT HRL Gen-IV (b).

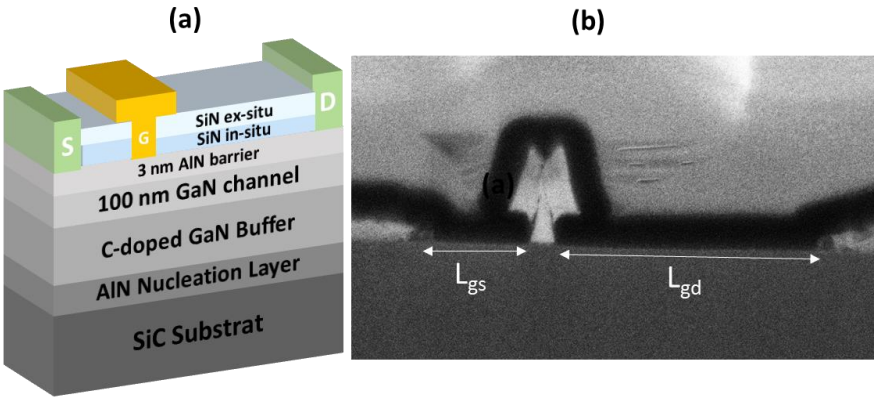

Figure 3.19 Schematic cross section of an AlN/GaN HEMT (a) and FIB view of a 110 nm T-gate (b).

Figure 3.19a represents a schematic cross section of an AlN/GaN HEMT structure based on a 3 nm AlN barrier grown on GaN/SiC substrate. The HEMT was capped with 10 nm in-situ SiN layer used both as early passivation as well as to reduce trapping effects. The T-gate length shown in Figure 3.19b was 110 nm and 3 different L_{gd} of 0.5, 1.5 and 2.5 µm yielding high breakdown voltage of 50V, 100V and 130V respectively. F_t/F_{max} of 63/300 GHz are achieved at V_{ds} = 20V for L_g = 110 nm and L_{gd} = 0.5 µm. The F_t/F_{max} ratio close to 5 is attributed to the highly favorable aspect ratio: gate length / gate-to-channel distance (>25). Large signal characterizations have been carried out in Q-band and W-band. Figure 3.20a shows typical pulsed power performances at 40 GHz of a 2×50 µm transistor with L_{gd} = 1.5 µm. a saturated output power of 5.3 W/mm with a peak PAE above 60% at V_{ds} = 30V and around 50% with a saturated output power of 8.3 W/mm at V_{ds} = 40V. Despite the residual trapping effects, a high PAE around 50% up to V_{ds} = 40V is obtained in CW mode as shown in Figure 3.20b. Furthermore, CW large signal characterization at 94 GHz have then been performed on the same devices. A high output power of 4W/mm is obtained with a PAE of 14.3% at V_{ds} = 20V (Figure 3.21) [50].

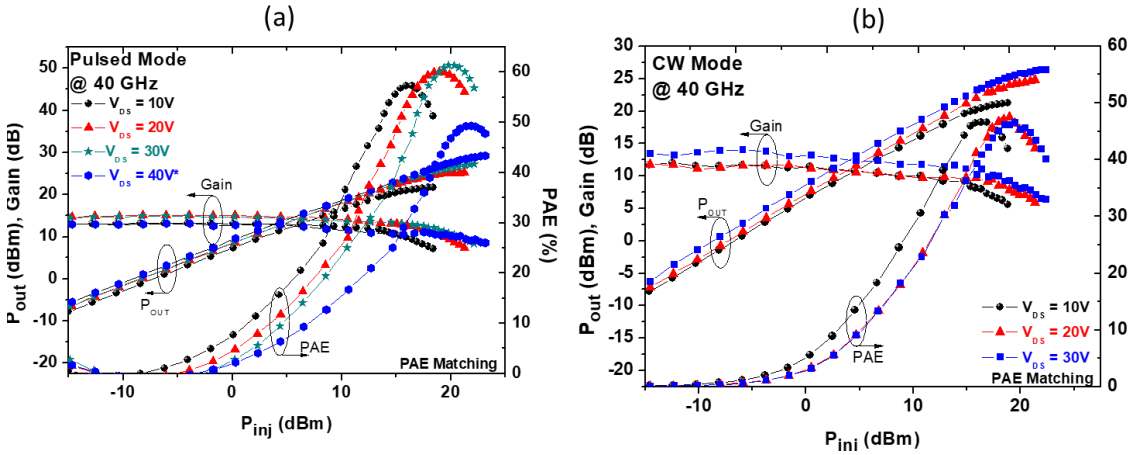

Figure 3.20 Pulsed (a) and CW (b) power performances of a 2×50 µm AlN/GaN HEMT (L_G = 110 nm, GD = 1.5µm) at V_{DS} = 10V, 20V, 30V and 40V*. **Power matching only*

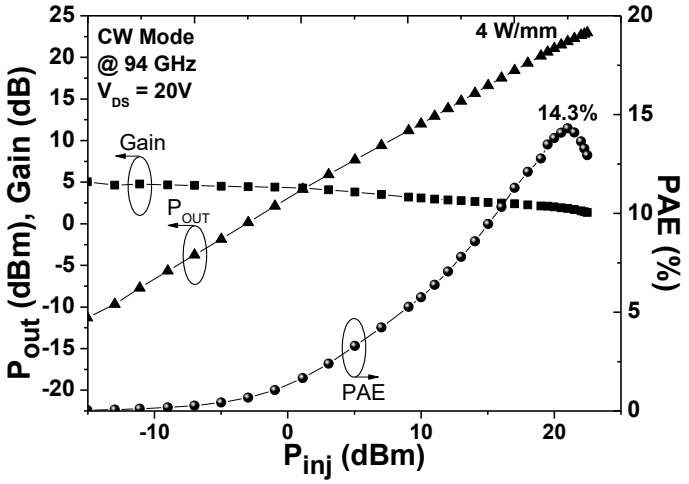

Figure 3.21 CW power performances of an AlN/GaN HEMT 2x25 µm with L_G = 110 nm for GD = 0.5µm at V_{DS} = 20V.

- InAlGaN-based device performances

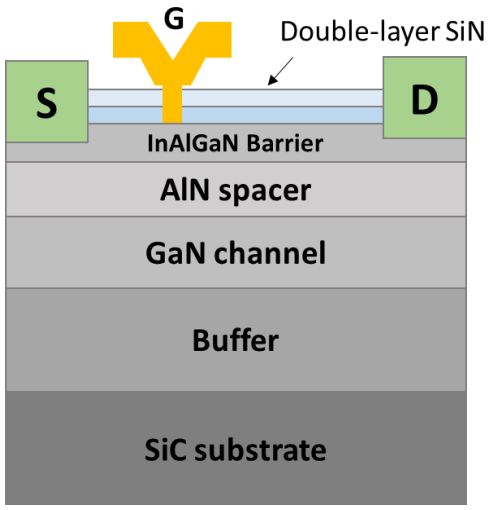

Figure 3.22 Device cross section of an InAlGaN/GaN HEMT.

Figure 3.22 shows the cross section of Fujitsu's 80 nm gate length InAlGaN/GaN HEMT technology. InAlGaN barrier was used to avoid the formation of surface pits thus reducing the gate leakage current (I_g) as compared to the ternary InAlN, which is required to improve the breakdown voltage and device reliability [49]. In addition, InAlGaN barrier is well known for its high 2DEG density combined to a high electron mobility. A double SiN passivation layer has been used to eliminate the current collapse. The offset overhanging gate was adopted to decrease the electric field without degrading high frequency performances. Load-pull measurements at 96 GHz show high output power of 3.0 W/mm at V_{ds} = 20V under pulsed mode operation. Besides, an improved 80 nm gate length InAlGaN/GaN HEMT demonstrated high power operation in the wide-

frequency range from S to W-band, using regrown n+ GaN contact layer, an InGaN back barrier to reduce off-state drain leakage current and an AlGaN spacer layer to realize high 2DEG close to 2×10^{13} cm^{-2}. Moreover, a diamond heat spreader was introduced in order to decrease the thermal resistance and further improve the output power density. The maximum pulsed output power density of this InAlGaN/GaN MMIC amplifier was 4.5 W/mm at 94 GHz [95]. It is intended that this power amplifier can be used in wireless backhaul communications.

4.2. State-of-the-Art mm-Wave GaN transistors

Figure 3.23 shows a benchmark of PAE as a function of P_{OUT} for GaN HEMTs in the mmW range up to W-band. In 2005, *T. Palacios et al.* reported a record Q-band P_{OUT} of 10.5 W/mm with a PAE of 33% at 40 GHz using AlGaN/GaN HEMT technology with L_g = 160 nm, where the PAE was limited mainly because of the linear gain of 6 dB [96]. J. *S. Moon et al.* reported gate recessed and field plated AlGaN/GaN HEMT at 30 GHz with a P_{OUT} of 5.7 W/mm associated to a PAE of 45% [97]. Also at 40 GHz, *F. Medjdoub et al*. demonstrated in pulsed mode AlN/GaN HEMT an outstanding PAE of 65% at V_{DS} = 10V with a high P_{OUT} of 8.3 W/mm at V_{DS} = 40V [50]. Hence, compared to other technologies, much higher efficiency and P_{OUT} can be achieved with GaN HEMTs up to W-band and certainly beyond. Many efforts have been made in order to satisfy W-band requirements such as a short gate length (deep sub-100 nm), high F_t/F_{max} and low contact resistances. *Micovic et al*. from HRL reported the first W-band GaN transistors with high performance in 2006 (14% efficiency and 2.1 W/mm P_{OUT}) [98]. *Mikiyama et al*. from Fujitsu labs developed 80 nm Schottky-gate InAlGaN/GaN HEMT which provides more than 3 W/mm high power density at 96 GHz [49]. Recently, *F. Medjdoub et al*. demonstrated a state of the art P_{OUT} of 4 W/mm at 94 GHz associated to a PAE of 14% using AlN/GaN HEMT technology [50]. While these conventional GaN HEMT structures are developed on Ga-polar hetero-structures, recent research from UCSB has shown the emergence of N-polar hetero-structures providing 28% efficiency with a P_{OUT} of 8 W/mm at 94 GHz [92]. It can be pointed out that the optimum technology choice is not based only on performances but also on the device reliability under harsh conditions. This will determine in a near future which GaN-based structure will be best suited for mmW applications.

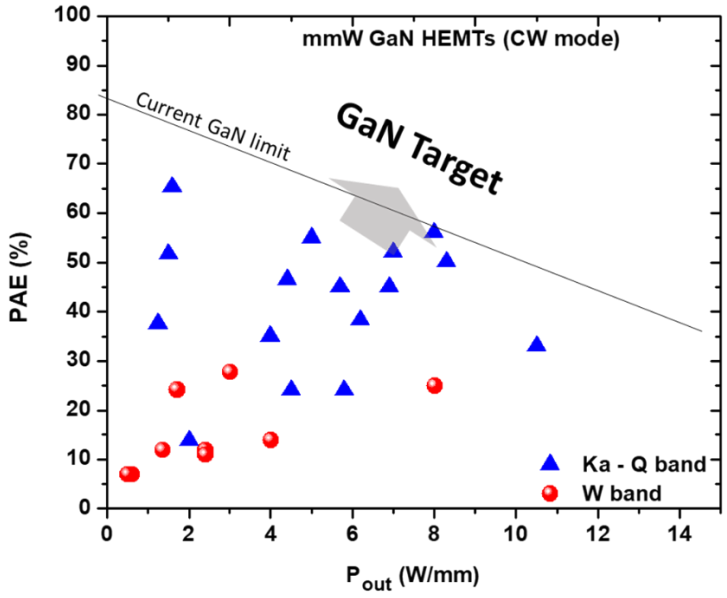

Figure 3.23 Benchmark of PAE as a function of P_{OUT} for mmW GaN HEMTs.

5. Overview of MMIC powers amplifiers

5.1. MMIC technology using III-N Devices

- *III-V materials based MMICs technology*

MMICs, based on III-V semiconductors technology are one of the key building block to meeting the requirements for mmW applications. Monolithic means that the full fabricated circuit is built on a single piece of a semiconductor material such as GaAs, InP, SiGe or GaN resulting in highly integrated and compact devices. Although high performance mmW GaAs and InP based MMICs have been reported so far, the increasing bandwidth and power requirements for mmW applications are limited with these traditional semiconductor technologies. GaN is a potential solution to satisfy the RF mmW transmitter requirements for communications and SATCOM applications [43]. For instance, GaN devices are being used in harsh environment receiver applications owing to its low noise performances and robustness. Therefore, GaN-based can cover any MMIC functions such as mixing, low noise amplification, power amplification and high frequency switching. Figure 3.24 shows an example of typical elements in RF transmit and receive modules in wireless communications. There are two key components inside the transmit/receive module, which are the power amplifiers (PA) and low noise amplifiers (LNA). In addition to these components there are different transmit/receive functions integrated in the mmW modules, including the oscillators, filters, linear mixers, converters and RF switches [99].

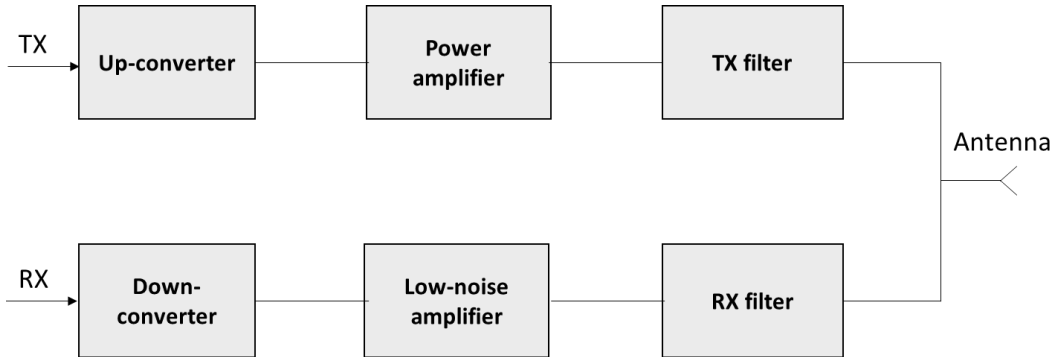

Figure 3.24 Schematic example of RF transmit/receive in communication base station.

Millimeter-wave MMIC systems need to deliver not only high performances but also low cost and compact size. Along with active devices, standard passive components such as metal-insulator-metal (MIM) capacitors, metal evaporated thin film resistors, bulk resistors and via holes are used for the circuit realization [100]. A number of foundries use specific techniques for the MMICs implementation such as grounded coplanar waveguide (GCPW), microstrip transmission lines technology and Cu damascene multi-layer process for 3D interconnection. Microstrip transmission lines are mostly used for MMICs and become more critical at higher frequency [101]. Cu damascene multi-layer process for 3D interconnection provides high power, high current and low-loss passive component [102]. The GCPW allows for low-inductive ground connection [103]. Moreover, CPW enables lower dispersion than microstrip technology for broadband applications as well as simple and cheaper fabrication because of the absence of via holes and backside processing, which is beneficial for mmW operation.

- *Power amplifiers*

Power amplifiers and circuits design are extensively investigated for mmW applications. The main challenges for next generation power MMICs are the achievement of a high output power up to at least 100 GHz combined with high PAE in order to reduce the power consumption.

Class-A, A/B and C for power amplifier GaN MMICs:

Power amplifiers are classified as linear class-A and non-linear A/B and C for analog design. Each class has its advantages and drawbacks as they typically generate trade-offs [99]. Class-A operation is the main class to provide high power density with better linearity but with a lower efficiency. Indeed, in class-A the quiescent drain current is fixed to the half of the maximum drain current leading to high power density and therefore significant power consumption [104]. Class-A/B operation is quite popular. The quiescent drain current is set to the optimum value corresponding to a trade-off between the linearity and efficiency. Finally, the class-C operation is also limited by the linearity, it is used typically for narrow band applications, in driver amplifier [105] and in rectifier mode to enhance efficiency [106].

Class D, E and F for Switch amplifier GaN MMICs:

Class D, E and F operations are used in switch mode GaN amplifiers in order to improve the efficiency. Class-D operation is typically used for amplifiers operating at low frequencies. Class-E amplifiers is designed to reduce the power loss during RF-switching. The ideal Class-E amplifier is a switched-mode circuit which combines zero dissipated power with zero voltage switching and zero derivative of voltage switching [107]. Class-E corresponds to a highly efficient tuned switching power amplifier. In Class-F amplifiers, harmonic tune technique was developed to further improve the performance beyond those of class-A, and A/B designs [108][109]. Therefore, Class-F amplifiers can operate at higher frequencies, but are limited by the complexity of the circuit and the tuning requirements.

- *Low noise amplifier*

The noise performance of the first amplifier stage affects the receiver noise figure and thus its sensitivity. The aim of a low-noise amplifier (LNA) is to amplify the desired small powered signal from the antenna while minimizing the degradation of the signal-to-noise ratio. A LNA is located at the first stage in a RF receiver module and is a key element as its noise performance dominates in a cascaded RF receiver system. The figure of merits of an LNA include high gain (typically > 20 dB) and a low noise (NF) figure (< 2 dB) for higher linearity. GaN is also a promising candidate for reaching this overall figure of merits. They can provide a good sensitivity at low power input and a reasonable gain thus a good linearity at high power levels. Several LNAs based on GaN operating at various frequency have been reported. For Ka-band (27 GHz – 40 GHz), a NF as low as 1 dB measured at 37 GHz with 24 dB gain using GaN HEMTs T4-A generation of HRL technology [110]. In the frequency band (100 MHz – 45 GHz) a low noise gate-termination-less Cascode distributed amplifier GaN MMICs demonstrated 10 dB gain and 1.6-3 dB of NF from 130 MHz to 26 GHz [111]. At high frequency, a highly-linear LNA MMIC using AlGaN/GaN HEMTs technology reported 25 dB gain and 5.6 NF at 84 GHz [112]. The required NFs of the LNAs are in the range of 1 to 5 dB. GaN based LNA designs reported in the literature deliver lower NF in comparison to other technologies based on III-V materials, which proves that GaN is promising for next generation robust receiver design.

5.2. MMIC examples from Ka-band to D-band frequencies

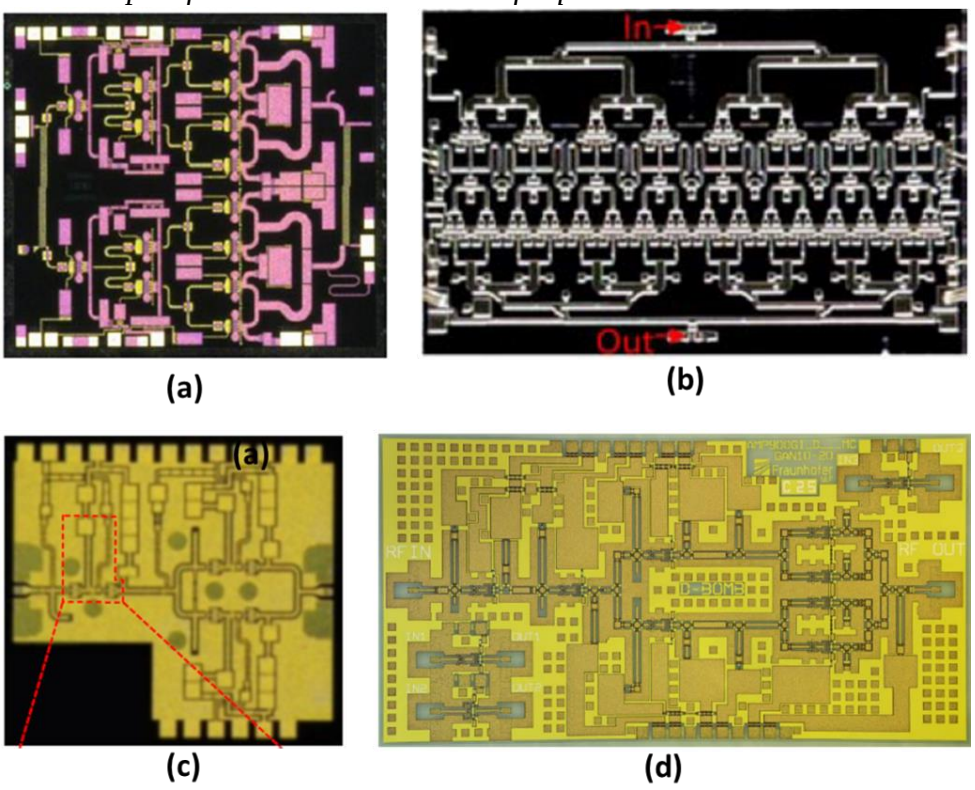

Figure 3.25 Examples of millimeter-wave MMICs at different frequencies: Ka-band (a)(b), W-band (c) and D-band (d).

Figure 3.25 provides examples of state-of-the art millimeter-wave GaN MMICs with different designs. Figure 3.25a shows an image of 3-stages Ka-band design [11] with a chip size of 1.74×3.24 mm². The MMIC technology is based on a 0.15 µm gate length AlGaN/GaN HEMTs fabricated on SiC. The measured results under CW operation for the balanced 3-stages demonstrate 9.5-11 W output power and 26-30% associated PAE between 28-31 GHz. For single-ended amplifier type, the measurement results show an output power of 5.8-6.4 W and 28-34% of PAE for similar frequency range. Figure 3.25b illustrates Ka-band 0.15 µm AlGaN/GaN HEMTs MMIC amplifier. The gate pitch was optimally designed to obtain the maximum output power. The designed amplifier is two-stage single-ended amplifier and the size is 3.8×6.2 mm². The achieved output power under CW operation is 20 W and the PAE is 19% at 26.5 GHz. In the frequency range of (26 – 28) GHz the output power is greater than 15 W with an associated PAE of 13% [36]. Figure 3.25c shows a fabricated W-band GaN PA MMICs using 80 nm InAlGaN/GaN HEMTs [13]. The MMIC consist of two-stage cascade units with two transistors each and identical gate lengths in order to provide high gain and low loss matching circuit. The size of the MMIC was 2×1.8 mm². CW large signal characteristics were carried out at 86 GHz. The maximum output power density was 3.6 W/mm with a PAE of 12.3% at V_{ds} = 20V. Figure 3.25d depicts a D-band PA MMICs using 100 nm T-gate AlGaN/GaN HEMTs. The S parameters of the active devices demonstrated an F_t of 100 GHz and an F_{max} around 300 GHz. The MMIC

consists of four actively matched cascode stages and the MMIC size was 3.75×2.0 mm². Large signal measurements show a maximum output power density of 1.4 W/mm at 120 GHz at V_{ds} = 15V with associated PAE of 11.5% [103].

6. Conclusions

Nowadays, GaN-based HEMT is becoming a critical technology for mmW applications. Due to the outstanding material properties, recent advanced GaN device design provided a sharp increase in performances including high power, high efficiency, reliability and compact size. These capabilities are ideally suited for numerous mmW power applications such as beam-forming technology for both 5G, 6G wireless networks and PAs MMIC for W-band frequency and beyond. Therefore, GaN will play a strong role in advanced RF and mmW applications including 5G and satellite communications. Thermal management, especially when using small component sizes, together with full control of surface and bulk traps will be the main challenge to ensure the required device reliability.

References

1. R. s. PENGELLY, and TURNER, J.A. (1976) Monolithic Broadband GaAs F. E. T. Amplifiers. *Electron. Lett.*, **12**, 10.

2. Aust, M. V, Sharma, A.K., Fordham, O., Grundbacher, R., To, R., Tsai, R.S., and Lai, R. (2006) A 2.8-W Q-Band High-Efficiency Power Amplifier. *IEEE J. Solid-State Circuits*, **41** (10), 2241–2247.

3. Kong, K.K., Nguyen, B., Nayak, S., and Kao, M. (2005) Ka-Band MMIC High Power Amplifier (4W at 30 GHz) with Record Compact Size. *IEEE Compd. Semicond. Integr. Circuit Symp.*, 232–235.

4. Campbell, C.F., Dumka, D.C., Kao, M., and Fanning, D.M. (2011) High Efficiency Ka-band Power Amplifier MMIC Utilizing a High Voltage Dual Field Plate GaAs PHEMT Process. *IEEE Compd. Semicond. Integr. Circuit Symp.*, 1–4.

5. Liu, S.M.J., Tang, O.S.A., Kong, W., Nichols, K., Heaton, J., Chao, P.C., Company, A.L.M., and Road, S.B. (1999) High Efficiency Monolithic InP HEMT V-band Power Amplifier. *IEEE Gall. Arsenide Integr. Circuit Symp.*, 145–147.

6. Chen, Y.C., Ingram, D.L., Lai, R., Barsky, M., Grunbacher, R., Block, T., Yen, H.C., and Streit, D.C. (1998) A 95-GHz InP HEMT MMIC Amplifier with 427-mW Power Output. *IEEE Microw. Guid. WAVE Lett. Microw. Guid. WAVE Lett.*, **8** (11), 399–401.

7. Chen, Y.C., Ingram, D.L., Yamauchi, D., Brunner, B., Kraus, J., Barsky, M., Grundbacher, R., Cha, S.K., Lai, R., Block, T., Wojtowicz, M., Chin, T.P., Allen, B., Yen, H.C., and Streit, D.C. (1999) A Single Chip 1-W InP HEMT V-Band Module. *IEEE Gall. Arsenide Integr. Circuit Symp.*, 149–152.

8. Fung, A., Ward, J., Chattopadhyay, G., Lin, R., Samoska, L., Kangaslahti, P., Mehdi, I., Lambrigtsen, B., Goldsmith, P., Micovic, M., Kurdoghlian, A., Shinohara, K., Milosavljevic, I., and Chow, D.H. (2011) Power Combined Gallium Nitride Amplifier with 3 Watt Output Power at 87 GHz. *IEEE J. Solid-State Circuits*, **41**.

9. Chavarkar, P.M., and Parikb, P. (2003) 3.5-Watt AlGaNlGaN HEMTs and Amplifiers at 35 GHz. *IEEE Int. Electron Devices Meet.*, 579–582.

10. Chen, S., Nayak, S., Campbell, C., and Reese, E. (2016) High Efficiency 5W / 10W 32 - 38GHz Power Amplifier MMICs Utilizing Advanced 0 . 15 µ m GaN HEMT Technology. *IEEE Compd. Semicond. Integr. Circuit Symp.*, 1–4.

11. Campbell, C.F., Liu, Y., Kao, M., and Nayak, S. (2013) High Efficiency Ka-Band Gallium Nitride Power Amplifier MMICs. *IEEE Int. Conf. Microwaves, Commun. Antennas Electron. Syst.*, 1–5.

12. Masuda, S., Ohki, T., Makiyama, K., Kanamura, M., Okamoto, N., and Shigematsu, H. (2009) GaN MMIC Amplifiers for W-band Transceivers. *Eur. Microw. Conf.*, 1796–1799.

13. Niida, Y., Kamada, Y., Ohki, T., Ozaki, S., Makiyama, K., Minoura, Y., Okamoto, N., Sato, M.,

Joshin, K., and Watanabe, K. (2016) 3 . 6 W / mm High Power Density W-band InAlGaN / GaN HEMT MMIC Power Amplifier. *IEEE Top. Conf. Power Amplifiers Wirel. Radio Appl.*, 24–26.

14. Micovic, M., Kurdoghlian, A., Shinohara, K., Burnham, S., Hu, I.M.M., Corrion, A., Fung, A., Lin, R., Samoska, L., Kangaslahti, P., Lambrigtsen, B., Goldsmith, P., Wong, W.S., Schmitz, A., Hashimoto, P., Willadsen, P.J., and Chow, D.H. (2010) W-Band GaN MMIC with 842 mW Output Power at 88 GHz. *IEEE MTT-S Int. Microw. Symp.*, 237–239.

15. Brown, A., Brown, K., Chen, J., Hwang, K.C., Kolias, N., and Scott, R. (2011) W-Band GaN Power Amplifier MMICs. *IEEE MTT-S Int. Microw. Symp.*, 1–4.

16. Brown, D.F., Williams, A., Shinohara, K., Kurdoghlian, A., Milosavljevic, I., Hashimoto, P., Burnham, S., Butler, C., Willadsen, P., and Micovic, M. (2011) W-Band Power Performance of AlGaN / GaN DHFETs with Regrown n + GaN Ohmic Contacts by MBE. *IEEE Int. Electron Devices Meet.*, 461–464.

17. Schwantuschke, D., Godejohann, B.J., Brückner, P., Tessmann, A., and Quay, R. (2018) mm-Wave Operation of AlN / GaN-Devices and MMICs at V- & W-band. *IEEE Int. Microw. Radar Conf.*, 238–241.

18. Brown, A., Brown, K., Chen, J., Gritters, D., and Hwang, K.C. (2012) High Power , High Efficiency E-Band GaN Amplifier MMICs. *IEEE Int. Conf. Wirel. Inf. Technol. Syst.*, 1–4.

19. Margomenos, A., Kurdoghlian, A., Micovic, M., Shinohara, K., Brown, D.F., Corrion, A.L., Laboratories, J.P., and Grove, O. (2014) GaN Technology for E , W and G-band Applications. *IEEE Compd. Semicond. Integr. Circuit Symp.*, 1–4.

20. Micovic, M., Kurdoghlian, A., Moyer, H.P., Hashimoto, P., Hu, M., Antcliffe, M., Willadsen, P.J., Wong, S., Bowen, R., Milosavljevic, I., Yoon, Y., Schmitz, A., Wetzel, M., Mcguire, C., Hughes, B., and Chow, D.H. (2008) GaN MMIC PAs for E-Band (71 GHz – 95 GHz) Radio. *IEEE Compd. Semicond. Integr. Circuit Symp.*, 1–4.

21. Schellenberg, J., Watkins, E., Micovic, M., Kim, B., and Han, K. (2010) W-band, 5W solid-state power amplifier/combiner. *IEEE MTT-S Int. Microw. Symp.*, 240–243.

22. Carrubba, V., Akmal, M., Quay, R., Lees, J., Benedikt, J., Cripps, S.C., and Tasker, P.J. (2012) The Continuous Inverse Class-F Mode With Resistive Second-Harmonic Impedance. *IEEE Trans. Microw. Theory Tech.*, **60** (6), 1928–1936.

23. Fung, A., Samoska, L., Kangaslahti, P., Lin, R., Mehdi, I., Sadowy, G., Tanelli, S., Peralta, A., Soria, M., Brown, A., Gritters, D., Connor, S.O., and Lardizabal, S. (2018) Gallium Nitride Amplifiers Beyond W-Band. *IEEE Radio Wirel. Symp.*, 150–153.

24. Schellenberg, J., Tran, A., Bui, L., Cuevas, A., and Watkins, E. (2016) 37 W , 75-100 GHz GaN Power Amplifier. *IEEE MTT-S Int. Microw. Symp.*, 81–84.

25. Dennler, P., Br, P., Schlechtweg, M., and Ambacher, O. (2014) Watt-Level Non-Uniform Distributed 6 – 37 GHz Power Amplifier MMIC with Dual-Gate Driver Stage in GaN

Technology. *IEEE Top. Conf. Power Amplifiers Wirel. Radio Appl.*, 37–39.

26. Dennler, P., Schwantuschke, D., and Ambacher, O. (2012) 8 – 42 GHz GaN Non-Uniform Distributed Power Amplifier MMICs in Microstrip Technology. *IEEE/MTT-S Int. Microw. Symp. Dig.*

27. IMT Vision – Framework and overall objectives of the future development of IMT for 2020 and beyond. Online. Available: *https://www.itu.int/dms_pubrec/itu-r/rec/m/R-REC-M.2083-0-201509-I!!PDF-E.pdf*.

28. 5G Semiconductor Solutions - Infrastructure and Fixed Wireless Access. June 2018. Online. Available: *https://www.qorvo.com/resources/d/5g-semiconductor-solutions-infrastructure-and-fixed-wireless-access-ebook*.

29. Nakatani, K., Yamaguchi, Y., Komatsuzaki, Y., and Shinjo, S. (2019) Millimeter-wave GaN Power Amplifier MMICs for 5G Application. *IEEE Int. Symp. Circuits Syst.*, 6–9.

30. Lie, D.Y.C., Mayeda, J.C., and Lopez, J. (2017) Highly Efficient 5G Linear Power Amplifiers (PA) Design Challenges. *Int. Symp. VLSI Des. Autom. Test*, 1–3.

31. Popovic, Z. (2017) Amping Up the PA for 5G: Efficient GaN Power Amplifiers with Dynamic Supplies. *IEEE Microw. Mag.*, **18** (3), 137–149.

32. Yuk, K., Branner, G.R., and Cui, C. (2017) Future Directions for GaN in 5G and Satellite Communications. *IEEE 60th Int. Midwest Symp. Circuits Syst.*, 803–806.

33. Pelk, M.J., Neo, W.C.E., Gajadharsing, J.R., Pengelly, R.S., and Vreede, L.C.N. De (2008) A High-Efficiency 100-W GaN Three-Way Doherty Amplifier for Base-Station Applications. *IEEE Trans. Microw. Theory Tech.*, **56** (7), 1582–1591.

34. Campbell, C.F., Tran, K., Kao, M., and Nayak, S. (2012) A K-Band 5W Doherty Amplifier MMIC Utilizing 0 . 15 µ m GaN on SiC HEMT Technology. *2012 IEEE Compd. Semicond. Integr. Circuit Symp.*, 1–4.

35. Micovic, M., Brown, D.F., Regan, D., Wong, J., Tang, Y., Herrault, F., Santos, D., Burnham, S.D., Tai, J., Prophet, E., Khalaf, I., Mcguire, C., Bracamontes, H., Fung, H., Kurdoghlian, A.K., and Schmitz, A. (2016) High Frequency GaN HEMTs for RF MMIC Applications. *IEEE Int. Electron Devices Meet.*, 3.3.1-3.3.4.

36. Yamaguchi, Y., Kamioka, J., Hangai, M., Shinjo, S., and Yamanaka, K. (2017) A CW 20W Ka-band GaN High Power MMIC Amplifier with a Gate Pitch Designed by Using One-Finger Large Signal Models. *IEEE Compd. Semicond. Integr. Circuit Symp. CSIC '05.*, 5–8.

37. Noh, Y., Choi, Y., and Yom, I. (2015) Ka-band GaN Power Amplifier MMIC Chipset for Satellite and 5G Cellular Communications. *IEEE 4th Asia-Pacific Conf. Antennas Propag.*, 453–456.

38. Nakatani, K., Yamaguchi, Y., Komatsuzaki, Y., and Sakata, S. (2018) A Ka-Band High Efficiency Doherty Power Amplifier MMIC using GaN-HEMT for 5G Application. *IEEE MTT-S Int. Microw. Work. Ser. 5G Hardw. Syst. Technol.*, 1–3.

39. Coffey, M., Momenroodaki, P., Zai, A., and Popovi, Z. (2015) A 4.2-W 10-GHz GaN MMIC Doherty Power Amplifier. *IEEE Compd. Semicond. Integr. Circuit Symp.*

40. Cheng, Q., Zhu, S., and Wu, H. (2013) Investigating the Global Trend of RF Power Amplifiers with the Arrival of 5G. *IEEE Int. Wirel. Symp. (IWS 2015)*, 1–4.

41. Tmoya, K., Kazumi, S., and Kunihiro, K. (2014) GaN HEMT High Efficiency Power Amplifiers for 4G/5G Mobile Communication Base Stations. *IEEE Asia-Pacific Microw. Conf.*, 6–9.

42. Zhang, Z., Xiao, Y., Ma, Z., Xiao, M., and Ding, Z. (2019) 6G Wireless Networks: Vision, Requirements, Architecture, and Key Technologies. *IEEE Veh. Technol. Mag.*, **14** (3), 28–41.

43. Runton, D.W., Trabert, B., Shealy, J.B., and Vetury, R. (2013) History of GaN. *IEEE Microw. Mag.*, **14** (3), 82–93.

44. Arulkumaran, S., and Vicknesh, S. (2013) Enhanced Breakdown Voltage With High Johnson ' s HEMTs on Silicon by (NH 4) 2 S x Treatment. *IEEE ELECTRON DEVICE Lett.*, **34** (11), 1364–1366.

45. Huang, S., Wei, K., Liu, G., Zheng, Y., Wang, X., Pang, L., Kong, X., Liu, X., Tang, Z., Yang, S., Jiang, Q., and Chen, K.J. (2014) High- fmax High Johnson's Figure-of-Merit 0.2-µm GateGate AlGaN / GaN HEMTs on Silicon Substrate With AlN / SiN x Passivation. *IEEE ELECTRON DEVICE Lett.*, **35** (3), 315–317.

46. Zanoni, E. GaN HEMT reliability research – a white paper –. 1–61.

47. Nayak, S., Kao, M., Chen, H., Smith, T., Goeller, P., Gao, W., Jimenez, J., Chen, S., Campbell, C., Drandova, G., Kraft, R., and Road, W.R. (2015) 0.15µm GaN MMIC Manufacturing Technology for 2-50 GHz Power Applications. *CS MANTECH Conf.*, 43–46.

48. Whelan, C.S., Kolias, N.J., Brierley, S., Macdonald, C., and Bernstein, S. (2012) GaN Technology for Radars. *CS MANTECH Conf.*

49. Makiyama, K., Ozaki, S., Ohki, T., Okamoto, N., Minoura, Y., Niida, Y., Kamada, Y., Joshin, K., Watanabe, K., and Miyamoto, Y. (2015) Collapse-Free High Power InAlGaN / GaN-HEMT with 3 W / mm at 96 GHz. *IEEE Int. Electron Devices Meet.*, 9.1.1-9.1.4.

50. Harrouche, K., Kabouche, R., Okada, E., and Medjdoub, F. (2019) High Performance and Highly Robust AlN / GaN HEMTs for Millimeter-Wave Operation. *IEEE J. Electron Devices Soc.*, **7**, 1145–1150.

51. Meneghesso, G., Verzellesi, G., Danesin, F., Rampazzo, F., Zanon, F., Tazzoli, A., Meneghini, M., and Zanoni, E. (2008) Reliability of GaN High-Electron-Mobility Transistors : State of the Art and Perspectives. *Ieee Trans. Device Mater. Reliab.*, **8** (2), 332–343.

52. Meneghesso, G., Meneghini, M., Tazzoli, A., Ronchi, N., Stocco, A., Chini, A., and Zanoni, E. (2010) Reliability issues of Gallium Nitride High Electron Mobility Transistors. *Int. J. Microw. Wirel. Technol.*, **2** (1), 39–50.

53. Ono, N., Senju, T., and Takagi, K. (2018) 53 % PAE 32W Miniaturized X-band GaN HEMT Power Amplifier MMICs. *Asia-Pacific Microw. Conf.*, 557–559.

54. Binari, S.C., Ikossi, K., Roussos, J.A., Kruppa, W., Park, D., Dietrich, H.B., Koleske, D.D., Wickenden, A.E., and Henry, R.L. (2001) Trapping Effects and Microwave Power Performance. *IEEE Trans. Electron Devices*, **48** (3), 465–471.

55. Binari, S.C., Klein, P.B., and Kazior, T.E. (2002) Trapping Effects in GaN and SiC Microwave FETs. *Proc. IEEE*, **90** (6), 1048–1058.

56. Vetury, R., Zhang, N.Q., Keller, S., and Mishra, U.K. (2001) The Impact of Surface States on the DC and RF Characteristics of AlGaN / GaN HFETs. *IEEE Trans. Electron Devices*, **48** (3), 560–566.

57. Mitrofanov, O., and Manfra, M. (2004) Mechanisms of gate lag in GaN / AlGaN / GaN high electron mobility transistors. *Superlattices Microstruct.*, **34** (2003), 33–53.

58. Faqir, M., Verzellesi, G., Chini, A., Fantini, F., Danesin, F., Meneghesso, G., Zanoni, E., and Dua, C. (2008) Mechanisms of RF Current Collapse in AlGaN – GaN High Electron Mobility Transistors. *IEEE Trans. DEVICE Mater. Reliab.*, **8** (2), 240–247.

59. Zhang, A.P., Rowland, L.B., Kaminsky, E.B., Tilak, V., Grande, J.C., Teetsov, J., Vertiatchikh, A., and Eastman, L.F. (2003) Correlation of Device Performance and Defects in AlGaN / GaN High-Electron Mobility Transistors. *J. Electron. Mater.*, **32** (5), 388–394.

60. Kim, H., Vertiatchikh, A., Thompson, R.M., Tilak, V., Prunty, T.R., Shealy, J.R., and Eastman, L.F. (2003) Hot electron induced degradation of undoped AlGaN / GaN HFETs. *Microelectron. Reliab.*, **43** (6), 823–827.

61. Kordoš, P., Donoval, D., Florovič, M., Kováč, J., and Gregušová, D. (2008) Investigation of trap effects in AlGaN/GaN field-effect transistors by temperature dependent threshold voltage analysis. *Appl. Phys. Lett*, **92** (5), 1–4.

62. Kabouche, R., Pecheux, R., Harrouche, K., Okada, E., Medjdoub, F., Derluyn, J., Degroote, S., Germain, M., Gucmann, F., Middleton, C., Pomeroy, J.W., and Kuball, M. (2019) High Efficiency AlN/GaN HEMTs for Q-Band Applications with an Improved Thermal Dissipation. *Int. J. High Speed Electron. Syst.*, **28** (1–2).

63. Meneghesso, G., Chini, A., Zanoni, E., Manfredi, M., Pavesi, M., Boudart, B., and Gaquiere, C. (2000) Diagnosis of trapping phenomena in GaN MESFETs. *Int. Electron Devices Meet.*, 389–392.

64. Haruyama, J., Negishi, H., Nishimura, Y., and Nashimoto, Y. (1997) Substrate-Related Kink Effects with a Strong Light-Sensitivity in AlGaAs/InGaAs PHEMT. *IEEE Trans. Electron Devices*, **44** (1), 25–33.

65. Wang, M., and Chen, K.J. (2011) Kink Effect in AlGaN / GaN HEMTs Induced by Drain and Gate Pumping. *IEEE Electron Device Lett.*, **32** (4), 482–484.

66. Mazzanti, A., Verzellesi, G., Canali, C., Meneghesso, G., and Zanoni, E. (2002) Physics-Based

Explanation of Kink Dynamics in AlGaAs / GaAs HFETs. *IEEE Electron Device Lett.*, **23** (7), 383–385.

67. Sun, H.F., and Bolognesi, C.R. (2007) Anomalous behavior of heterostructure field-effect transistors at cryogenic temperatures : From current collapse to current enhancement with cooling Anomalous behavior of AlGaN / GaN heterostructure field-effect. *Appl. Phys. Lett*, **90** (12).

68. Lin, C., Wang, W., Lin, P., Lin, C., Chang, Y., and Chan, Y. (2005) Transient Pulsed Analysis on GaN HEMTs at Cryogenic Temperatures. *IEEE ELECTRON DEVICE Lett.*, **26** (10), 710–712.

69. Green, B.M., Chu, K.K., Chumbes, E.M., Smart, J.A., Shealy, J.R., Eastman, L.F., and Fellow, L. (2000) The Effect of Surface Passivation on the Microwave Characteristics of Undoped AlGaN / GaN HEMT ' s. *IEEE ELECTRON DEVICE Lett.*, **21** (6), 268–270.

70. Fujimoto, H., Saito, W., Yoshioka, A., Nitta, T., Kakiuchi, Y., and Saito, Y. (2008) Wafer Quality Target for Current-Collapse-Free GaN-HEMTs in High Voltage Applications. *CS MANTECH Conf.*

71. Wu, Y., Saxler, A., Moore, M., Smith, R.P., Sheppard, S., Chavarkar, P.M., Wisleder, T., Mishra, U.K., and Parikh, P. (2004) 30-W / mm GaN HEMTs by Field Plate Optimization. *IEEE ELECTRON DEVICE Lett.*, **25** (3), 117–119.

72. Romanczyk, B., Guidry, M., Wienecke, S., Li, H., Ahmadi, E., Zheng, X., Keller, S., and Mishra, U.K. (2016) W-Band N-Polar GaN MISHEMTs with High Power and Record 27 . 8 % Effic i ency at 94 GHz. *IEEE Int. Electron Devices Meet.*, 67–70.

73. Hickman, A., Chaudhuri, R., Bader, S.J., Nomoto, K., Lee, K., Xing, H.G., and Jena, D. (2019) High Breakdown Voltage in RF AlN / GaN / AlN Quantum Well HEMTs. *IEEE Electron Device Lett.*, **40** (8), 1293–1296.

74. Smorchkova, I.P., L. Chen, T.M., Shen, L., Heikman, S., Moran, B., Keller, S., DenBaars, S.P., Speck, J.S., and Mishra, U.K. (2001) AlN / GaN and (Al , Ga) N / AlN / GaN two- dimensional electron gas structures grown by plasma-assisted molecular-beam epitaxy. *J. Appl. Phys.*, **90** (10), 5196–5201.

75. Cheng, K., Leys, M., Derluyn, J., Degroote, S., Xiao, D.P., and Lorenz, A. (2007) AlGaN / GaN HEMT grown on large size silicon substrates by MOVPE capped with in-situ deposited Si3N4. *J. Cryst. Growth*, **298**, 822–825.

76. Tadjer, M.J., Anderson, T.J., Hobart, K.D., Mastro, M.A., Hite, J.K., Caldwell, J.D., Picard, Y.N., Kub, F.J., and Jr, C.R.E. (2010) Electrical and Optical Characterization of AlGaN / GaN HEMTs with In Situ and Ex Situ Deposited SiN x Layers. *J. Electron. Mater.*, **39** (11), 2452–2458.

77. Eastman, L.F., Tilak, V., Smart, J., Green, B.M., Chumbes, E.M., Dimitrov, R., Kim, H., Ambacher, O.S., Weimann, N., Prunty, T., Murphy, M., Schaff, W.J., and Shealy, J.R. (2001) Undoped AlGaN / GaN HEMTs for Microwave Power Amplification. *IEEE Trans. Electron Devices*, **48** (3), 479–485.

78. Ambacher, O., Smart, J., Shealy, J.R., Weimann, N.G., Chu, K., Murphy, M., Schaff, W.J., Eastman, L.F., Dimitrov, R., Wittmer, L., Stutzmann, M., Rieger, W., and Hilsenbeck, J. (1999) Two-dimensional electron gases induced by spontaneous and piezoelectric polarization charges in N- and Ga-face AlGaN / GaN heterostructures. *J. Appl. Phys.*, **85** (6), 3222–3233.

79. Jessen, G.H., Fitch, R.C., Gillespie, J.K., Via, G., Crespo, A., Langley, D., Denninghoff, D.J., Trejo, M., Heller, E.R., and Algan, A. (2007) Short-Channel Effect Limitations on High-Frequency Operation of AlGaN / GaN HEMTs for T-Gate Devices. *IEEE Trans. Electron Devices*, **54** (10), 2589–2597.

80. Shinohara, K., Regan, D.C., Tang, Y., Corrion, A.L., Brown, D.F., Wong, J.C., Robinson, J.F., Fung, H.H., Schmitz, A., Oh, T.C., Kim, S.J., Chen, P.S., Nagele, R.G., Margomenos, A.D., and Micovic, M. (2013) Scaling of GaN HEMTs and Schottky Diodes for Submillimeter-Wave MMIC Applications. *IEEE Trans. Electron Devices*, **60** (10), 2982–2996.

81. Milosavljevic, I., Shinohara, K., Regan, D., Burnham, S., Corrion, A., Hashimoto, P., Wong, D., Hu, M., Butler, C., Schmitz, A., Willadsen, P.J., and Micovic, M. (2010) Vertically scaled GaN/AlN DH-HEMTs with regrown n+GaN ohmic contacts by MBE. *Device Res. Conf. - Conf. Dig. DRC*, **54**, 159–160.

82. Shinohara, K., Regan, D., Corrion, A., Brown, D., Tang, Y., Wong, J., Candia, G., Schmitz, A., Fung, H., Kim, S., and Micovic, M. (2012) Self-Aligned-Gate GaN-HEMTs with Heavily-Doped n + -GaN Ohmic Contacts to 2DEG. *Int. Electron Devices Meet.*, 27.2.1-27.2.4.

83. Chung, J.W., Hoke, W.E., Chumbes, E.M., Palacios, T., and We, A. (2010) AlGaN / GaN HEMT With 300-GHz f max. *IEEE ELECTRON DEVICE Lett.*, **31** (3), 195–197.

84. Shinohara, K., Corrion, A., Regan, D., Milosavljevic, I., Brown, D., Burnham, S., Willadsen, P.J., Butler, C., Schmitz, A., Wheeler, D., Fung, A., and Micovic, M. (2010) 220GHz f T and 400GHz f max in 40-nm GaN DH-HEMTs with Re-grown Ohmic. *Int. Electron Devices Meet.*, 30.1.1-30.1.4.

85. Lin, Y.K., Bergsten, J., Leong, H., Malmros, A., Chen, J.T., Chen, D.Y., Kordina, O., Zirath, H., Chang, E.Y., and Rorsman, N. (2018) A versatile low-resistance ohmic contact process with ohmic recess and low-temperature annealing for GaN HEMTs. *Semicond. Sci. Technol.*, **33** (9).

86. Buttari, D., Chini, A., Palacios, T., Coffie, R., Shen, L., Xing, H., Heikman, S., McCarthy, L., Chakraborty, A., Keller, S., and Mishra, U.K. (2003) Origin of etch delay time in Cl 2 dry etching of AlGaN/GaN structures. *Appl. Phys. Lett.*, **83** (23), 4779–4781.

87. Wong, M.H., Pei, Y., Palacios, T., Shen, L., Chakraborty, A., McCarthy, L.S., Keller, S., Denbaars, S.P., Speck, J.S., and Mishra, U.K. (2007) Low nonalloyed Ohmic contact resistance to nitride high electron mobility transistors using N-face growth. *Appl. Phys. Lett.*, **91** (23), 1–4.

88. Selvanathan, D., Zhou, L., Kumar, V., and Adesida, I. (2002) Low resistance Ti/Al/Mo/Au

Ohmic contacts for AlGaN/GaN heterostructure field effect transistors. *Phys. Status Solidi Appl. Res.*, **194** (2), 583–586.

89. Guo, J., Li, G., Faria, F., Cao, Y., Wang, R., Verma, J., Gao, X., Guo, S., Beam, E., Ketterson, A., Schuette, M., Saunier, P., Wistey, M., Jena, D., and Xing, H. (2012) MBE-regrown ohmics in InAlN HEMTs with a regrowth interface resistance of 0.05 Ωmm. *IEEE Electron Device Lett.*, **33** (4), 525–527.

90. Yue, Y., Hu, Z., Guo, J., Sensale-Rodriguez, B., Li, G., Wang, R., Faria, F., Fang, T., Song, B., Gao, X., Guo, S., Kosel, T., Snider, G., Fay, P., Jena, D., and Xing, H. (2012) InAlN/AlN/GaN HEMTs with regrown ohmic contacts and f T of 370 GHz. *IEEE Electron Device Lett.*, **33** (7), 988–990.

91. Wienecke, S., Romanczyk, B., Guidry, M., Li, H., Ahmadi, E., Hestroffer, K., Zheng, X., Keller, S., and Mishra, U.K. (2017) N-Polar GaN Cap MISHEMT With Record Power Density Exceeding 6.5 W/mm at 94 GHz. *IEEE Electron Device Lett.*, **38** (3), 359–362.

92. Romanczyk, B., Wienecke, S., Guidry, M., Li, H., Ahmadi, E., Zheng, X., Keller, S., and Mishra, U.K. (2018) Demonstration of Constant 8 W/mm Power Density at 10, 30, and 94 GHz in State-of-the-Art Millimeter-Wave N-Polar GaN MISHEMTs. *IEEE Trans. Electron Devices*, **65** (1), 45–50.

93. Tang, Y., Shinohara, K., Regan, D., Corrion, A., Brown, D., Wong, J., Schmitz, A., Fung, H., Kim, S., and Micovic, M. (2015) Ultrahigh-speed GaN high-electron-mobility transistors with fT/fmax of 454/444 GHz. *IEEE Electron Device Lett.*, **36** (6), 549–551.

94. Moon, J., Wong, J., Grabar, B., Antcliffe, M., Chen, P., Arkun, E., Khalaf, I., and Corrion, A. (2019) High-speed Linear GaN Technology with a record Efficiency in Ka-band. *EUMW Conf.*

95. Kotani, J., Yamada, A., Ohki, T., Minoura, Y., Ozaki, S., Okamoto, N., Makiyama, K., and Nakamura, N. (2018) Recent advancement of GaN HEMT with InAlGaN barrier layer and future prospects of AlN-based electron devices. *IEEE Int. Electron Devices Meet.*, 30.4.1-30.4.4.

96. Palacios, T., Member, S., Chakraborty, A., Rajan, S., Poblenz, C., Keller, S., Denbaars, S.P., Member, S., Speck, J.S., and Mishra, U.K. (2005) High-Power AlGaN / GaN HEMTs for Ka-Band Applications. *IEEE ELECTRON DEVICE Lett.*, **26** (11), 781–783.

97. Moon, J.S., Wu, S., Wong, D., Milosavljevic, I., Conway, A., Hashimoto, P., Hu, M., Antcliffe, M., and Micovic, M. (2005) Gate-Recessed AlGaN – GaN HEMTs for High-Performance Millimeter-Wave Applications. *IEEE ELECTRON DEVICE Lett.*, **26** (6), 348–350.

98. Micovic, M., Kurdoghlian, A., Hashimoto, P., Hu, M., Antcliffe, M., Willadsen, P.J., Wong, W.S., Bowen, R., Milosavljevic, I., Schmitz, A., Wetzel, M., and Chow, D.H. (2006) GaN HFET for W-band Power Applications. *Int. Electron Devices Meet.*, 5–7.

99. Quay, R. (2014) *Group III-Nitride Monolithically Microwave Integrated Circuits (MMICs)*.

100. Pengelly, R.S., Wood, S.M., Milligan, J.W., Sheppard, S.T., and Pribble, W.L. (2012) A Review of GaN on SiC High Electron-Mobility Power Transistors and MMICs. *IEEE Trans. Microw. Theory Tech.*, **60** (2), 1764–1783.

101. Kolias, N.J., Whelan, C.S., Kazior, T.E., Smith, K. V, and Company, R. (2010) GaN technology for microwave and millimeter wave applications. *IEEE MTT-S Int. Microw. Symp.*, 1222–1225.

102. Margomenos, A., Micovic, M., Butler, C., Holden, B.T., Chang, D.T., Mcguire, C., and Chow, D.H. (2013) Low Loss , Cu Damascene Interconnects and Passives Compatible with GaN MMIC. *IEEE MTT-S Int. Microw. Symp. Dig.*, 1–4.

103. Maciej Cwiklinski, Brückner, P., Leone, S., Friesicke, C., Maßler, H., Lozar, R., Wagner, S., Quay, R., Member, S., and Ambacher, O. (2019) D-Band and G-Band High-Performance. *IEEE Trans. Microw. Theory Tech.*, 1–10.

104. Inoue, K., Sano, S., Tateno, Y., Yamaki, F., Ebihara, K., Ui, N., Kawano, A., and Deguchi, H. (2010) Development of Gallium Nitride High Electron Mobility Transistors for Cellular Base Stations. *SEI Tech. Rev.*, 88–93.

105. Santhakumar, R., Thibeault, B., Member, S., Higashiwaki, M., Keller, S., Chen, Z., Mishra, U.K., and York, R.A. (2011) Two-Stage High-Gain High-Power Distributed Amplifier Using Dual-Gate GaN HEMTs. *IEEE Trans. Microw. Theory Tech.*, **59** (8), 2059–2063.

106. Litchfield, M., Schafer, S., Reveyrand, T., and Popovic, Z. (2014) High-Efficiency X-Band MMIC GaN Power Amplifiers Operating as Rectifiers. *IEEE MTT-S Int. Microw. Symp.*, 1–4.

107. Kee, S.D., Aoki, I., Hajimiri, A., and Rutledge, D. (2003) The Class-E / F Family of ZVS Switching Amplifiers. *IEEE Trans. Microw. Theory Tech.*, **51** (6), 1677–1690.

108. Senju, T., Takagi, K., and Kimura, H. (2018) A 2 W 45 % PAE X-Band GaN HEMT Class-F MMIC Power Amplifier. *Asia-Pacific Microw. Conf.*, 956–958.

109. Gao, S., Xu, H., Mishra, U.K., and Barbara, S. (2006) MMIC class-F power amplifiers using field-plated AlGaN/GaN HEMTs. *IEEE Compd. Semicond. Integr. Circuit Symp.*

110. Micovic, M., Brown, D., Regan, D., Wong, J., Tai, J., Kurdoghlian, A., Herrault, F., Tang, Y., Burnham, S.D., Fung, H., Schmitz, A., Khalaf, I., Santos, D., Prophet, E., Bracamontes, H., Mcguire, C., and Grabar, R. (2016) Ka-band LNA MMIC ’s realized in f max > 580 GHz GaN HEMT Technology. *IEEE Compd. Semicond. Integr. Circuit Symp.*, 1–4.

111. Kobayashi, K.W., Denninghoff, D., and Miller, D. (2015) A Novel 100 MHz-45 GHz GaN HEMT Low Noise Non-Gate- Terminated Distributed Amplifier based on a 6-inch 0 . 15 m GaN-SiC mm-Wave Process Technology. *2015 IEEE Compd. Semicond. Integr. Circuit Symp.*, 1–4.

112. Masslerl, H., Wagnerl, S., and Brucknerl, P. (2011) A Highly Linear 84 GHz Low Noise Amplifier MMIC In AlGaN/GaN HEMT Technology 1. *IEEE MTT-S Int. Microw. Work. Ser. Millim. Wave Integr. Technol.*, 144–147.